European Journal of Phycology

ISSN: (Print) (Online) Journal homepage: https://www.tandfonline.com/loi/tejp20

Clarifying confusion – *Prorocentrum triestinum* J.Schiller and *Prorocentrum redfieldii* Bursa (Prorocentrales, Dinophyceae) are two different species

Urban Tillmann, Alfred Beran, Marc Gottschling, Stephan Wietkamp & Mona Hoppenrath

To cite this article: Urban Tillmann, Alfred Beran, Marc Gottschling, Stephan Wietkamp & Mona Hoppenrath (2022) Clarifying confusion – *Prorocentrum triestinum* J.Schiller and *Prorocentrum redfieldii* Bursa (Prorocentrales, Dinophyceae) are two different species, European Journal of Phycology, 57:2, 207-226, DOI: 10.1080/09670262.2021.1948614

To link to this article: https://doi.org/10.1080/09670262.2021.1948614

EUROPEAN JOURNAL OF PHYCOLOGY
2022, VOL. 57, NO. 2, 207–226
https://doi.org/10.1080/09670262.2021.1948614

Clarifying confusion – *Prorocentrum triestinum* J.Schiller and *Prorocentrum redfieldii* Bursa (Prorocentrales, Dinophyceae) are two different species

Urban Tillmann [a], Alfred Beran [b], Marc Gottschling [c], Stephan Wietkamp [a] and Mona Hoppenrath [d]

[a]Alfred Wegener Institute for Polar and Marine Research, Am Handelshafen 12, D – 27570, Bremerhaven, , Germany; [b]Istituto Nazionale di Oceanografia e di Geofisica Sperimentale – Department of Oceanography, via Piccard 54, I – 34151 S. Croce,Trieste, Italy; [c]Department Biologie, Systematik, Biodiversität & Evolution der Pflanzen, GeoBio-Center, Ludwig-Maximilians-Universität München, Menzinger Str. 67, D – 80638 München, Germany; [d]Senckenberg am Meer, German Centre for Marine Biodiversity Research (DZMB), Südstrand 44, D – 26382 Wilhelmshaven, Germany

ABSTRACT

The Prorocentrales are a unique group of dinophytes based on several apomorphic traits, but species delimitation is challenging within the group. *Prorocentrum triestinum* was described by Josef Schiller in 1918 as an important bloom-forming species from Trieste (Mediterranean, Adriatic Sea) with a conspicuous asymmetric outline and a small, asymmetrically located subapical spine. All subsequent records under this name fail to conform to Schiller's original description. These inconsistencies have their origin in John Dodge's 1975 revision of *Prorocentrum*, which placed *Prorocentrum redfieldii*, a more symmetrical, slender species with a long apical spine, into synonymy under *P. triestinum*. To clarify this confusion, we collected samples at the type locality of *P. triestinum* in Trieste and established a strain that is morphologically consistent with the protologue and suitable for use in epitypification. Morphology and rRNA sequence data of this strain were compared with four new strains identified as *P. redfieldii* from the Mediterranean Sea and the North Atlantic Ocean. Cells of *P. triestinum* had an asymmetric outline in lateral view and a small, dorso-subapical spine. These features, which are readily resolved by light microscopy, were distinct from those of the nearly symmetrical and slender cells of *P. redfieldii*, which had a long, apically located spine. The species are nevertheless closely related and share an identical architecture of the periflagellar area with a distinctive, largely reduced accessory pore together with a very small platelet 7. This apomorphy clearly differentiates both species from other species of *Prorocentrum*. Both species differ in their primary rRNA sequences, and ITS and LSU sequence differences will enable them to be distinguished in future meta-barcoding studies. The present study demonstrates that *P. triestinum* and *P. redfieldii* are distinct species and thus contributes to a reliable biodiversity assessment of *Prorocentrum*.

HIGHLIGHTS

- *Prorocentrum triestinum* is characterised molecularly for the first time and delimited from *P. redfieldii*.
- The identity of important bloom-forming species is clarified.
- Structural details of the periflagellar area are described.

ARTICLE HISTORY Received 17 January 2021; Revised 2 June 2021; Accepted 19 June 2021

KEYWORDS Diversity; epitypification; marine; Mediterranean Sea; microalgae; North Atlantic; phylogeny

Introduction

Species of the thecate dinophyte taxon *Prorocentrum* Ehrenberg are abundant elements of planktonic and benthic protist communities predominantly in marine waters worldwide (Dodge, 1975; Hoppenrath *et al.*, 2013). They are characterised by apical insertion of both flagella and the absence of a cingulum and sulcus. Cells are often laterally compressed with only two large lateral thecal plates. A number of minute platelets are arranged apically around a large flagellar pore and an accessory pore that is usually smaller (Hoppenrath *et al.*, 2013; Tillmann *et al.*, 2019). A number of planktonic species, such as *P. micans* Ehrenberg, *P. cordatum* (Ostenfeld) J.D.Dodge [= *P. minimum* (Pavillard) J. Schiller (Velikova & Larsen, 1999)] or *P. obtusidens* J. Schiller [= *P. donghaiense* D.Lu (Shin *et al.*, 2019)] form dense blooms in coastal waters (Heil *et al.*, 2005; Shin *et al.*, 2019; Tillmann *et al.*, 2019). Benthic or epiphytic species were poorly studied before the 1990s, when some were identified as a source of okadaic acid and other diarrhetic shellfish toxins (Yasumoto *et al.*, 1987; Hoppenrath *et al.*, 2014). A large number of new benthic *Prorocentrum* species have been subsequently recognised (Hoppenrath *et al.*, 2013; Chomérat *et al.*, 2019).

Most planktonic species of *Prorocentrum* were described in the early years of the 20th century solely based on light microscopic observations of cell morphology. Between 1918 and 1932, 20 planktonic species of *Prorocentrum* were described by Josef Schiller, who thus was responsible for the significant increase of the species number from five (Paulsen, 1908) to 39 (Schiller, 1937). Whilst working at the Trieste Zoological Station on Mediterranean planktonic protists, Schiller (1918) described *Prorocentrum triestinum*

CONTACT Urban Tillmann Urban.Tillmann@awi.de; Mona Hoppenrath mona.hoppenrath@senckenberg.de

Published online 07 Sep 2021

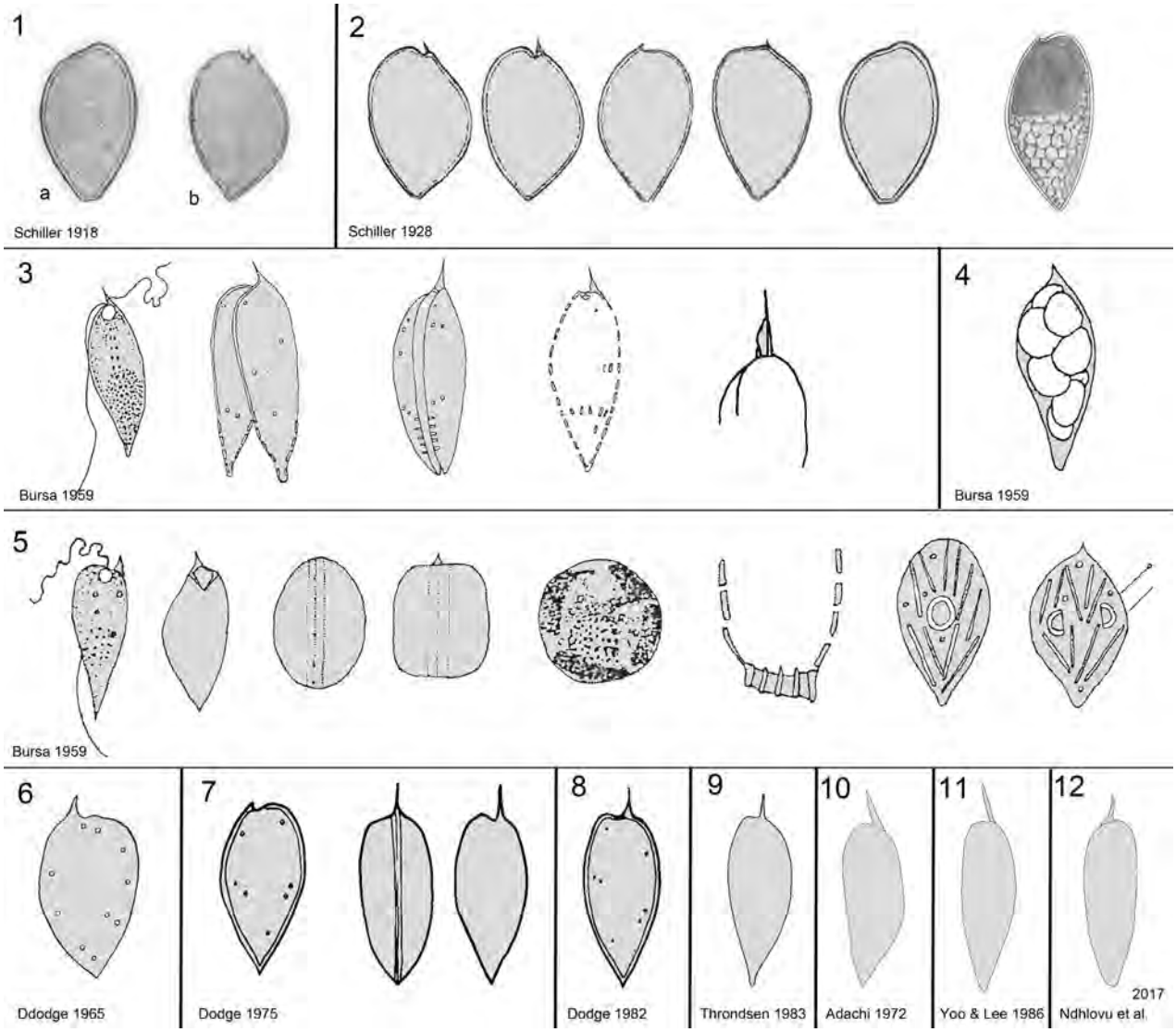

Figs 1–12. Line drawings of *Prorocentrum triestinum* and related species from the literature. **Fig. 1**. *P. triestinum* (redrawn after Schiller, 1918); a and b correspond to Schiller's denominations of his sub-figures; note that Schiller's fig. 1b is chosen here as lectotype). **Fig. 2**. *P. triestinum* (redrawn after Schiller, 1928). **Fig. 3**. *P. redfieldii* (redrawn after Bursa, 1959). **Fig. 4**. *P. triestinum* (redrawn after Bursa, 1959). **Fig. 5**. *P. pyrenoideum* (redrawn after Bursa, 1959). **Fig. 6**. *P. triestinum* (redrawn after Dodge, 1965). **Fig. 7**. *P. triestinum* (redrawn after Dodge, 1975). **Fig. 8**. *P. triestinum* (redrawn after Dodge, 1982). **Fig. 9**. *P. triestinum* (redrawn after Throndsen, 1983). **Fig. 10**. *P. triestinum* (redrawn after Adachi, 1972). **Fig. 11**. *P. triestinum* (redrawn after Yoo & Lee, 1986). **Fig. 12**. *P. triestinum* (redrawn after Ndhlovu *et al*., 2017).

J.Schiller as a small species (length 18–22 µm) with an asymmetric and in lateral view oblique outline of the cells; pores are very delicate and only faintly visible (his two drawings are here reproduced in Fig. 1). Schiller also emphasised the short and solid spine located on a tooth-like bump in a distinctly subapical position opposite an elevated apical-ventral part. He noted that *P. triestinum* formed massive blooms in Trieste harbour during summer and autumn, but that it was rare in the open Adriatic Sea (Schiller, 1918).

Considering the characteristic shape of *P. triestinum*, it is difficult to understand why subsequent records under its name (e.g. Adachi, 1972; Yoo & Lee, 1986; Ndhlovu *et al*., 2017) do not conform with Schiller's original descriptions and drawings. Confusion probably results from the first major revision of *Prorocentrum* by Dodge (1975), which was undertaken when the number of described species had increased to 64. Culture observations (mainly based on strains of *P. micans*: Braarud & Rossavik, 1951; Bursa, 1962) indicated large intraspecific variability in size and shape. Dodge (1975) consequently argued for broad circumscriptions of individual species to allow for variation in morphology. Thus, Dodge (1975) drastically reduced the number of species by extensive synonymisation, including that of *Prorocentrum redfieldii* Bursa and *Prorocentrum pyrenoideum* Bursa under *P. triestinum*.

Prorocentrum redfieldii was described by Adam S. Bursa in 1959 as a neritic, brackish species collected from coastal plankton near Woods Hole (Massachusetts, USA). Bursa's drawings (reproduced as Fig. 3) and descriptions show elongated cells with

a distinct and large spine in almost mid-apical position, and the presence of only a few thecal pores on otherwise smooth plates. In describing affinities, Bursa (1959: p. 19) stated that: 'It seems to be closely related to *P. triestinum* and *P. schilleri*', but he did not provide further explanation. The proposed affinity is difficult to understand, because one drawing labelled as *P. triestinum* (Bursa, 1959: fig. 117, here reproduced as Fig. 4) does not correspond to Schiller's original description.

The second synonymised species, namely *Prorocentrum pyrenoideum*, is more difficult to evaluate, because Bursa's drawings show cells with very different shapes (Fig. 5). The description was based on a strain isolated by Mary Parke in 1949 near Plymouth, UK (strain designation not explicitly stated in the species description, but likely to be '*Exuviaella* sp. No. 18', as is listed in the Materials and methods section). *Prorocentrum pyrenoideum* is characterized by the presence of a large central pyrenoid (lacking in *P. redfieldii* and *P. triestinum*), a prominent apical spine and uniquely shaped antapical tubular pores. For *P. pyrenoideum*, Bursa (1959: p. 19) also stated (again without further explanation) that 'its closest relative seems to be *P. triestinum*'. Dodge (1975) noted that Bursa's description of *P. pyrenoideum* was based on the Plymouth strain, which Dodge himself identified as *P. triestinum*, but without any description, drawing or micrograph of this particular strain.

In any case, both *P. redfieldii* and *P. pyrenoideum*, with their obviously longer spine and the generally slender shape, appear to be rather distinct from Schiller's *P. triestinum*. Dodge's motivation for synonymisation of both names under *P. triestinum* thus remains obscure but may rely on his early work on another strain of *Prorocentrum*, which also originated from Plymouth and was designated L.M. 1136-2 in the Cambridge Culture Collection (Dodge, 1965; Dodge & Crawford, 1970; Dodge & Bibby, 1973). Dodge identified this strain as *P. triestinum*, despite evidence that its cell shape and the spine length and position (see Fig. 6) deviated significantly from Schiller's description. Dodge (1965: p. 609) briefly described the thecal plates as follows: 'The … valves … had a completely smooth even surface … perforated by about ten trichocyst pores with thickened rims … dispersed around the margin' and mentioned that 'The apical spine was seen to vary considerably in size'. These observations may have convinced Dodge (1975) to depict two different cells as *P. triestinum* (Fig. 7), one obviously inspired by Schiller's drawing (although more slender in shape) but the other with a distinctly longer mid-apical spine. Notably, only one drawing of a slender cell with a long spine is reproduced as *P. triestinum* in Dodge's (1982) comprehensive field guide of marine dinoflagellates of the British Isles (Fig. 8). This morphology, a slender cell with a long spine, corresponds to *P. redfieldii* as described by Bursa (1959) and has been widely adopted (see Adachi, 1972; Throndsen, 1983; Yoo & Lee, 1986; Ndhlovu *et al.*, 2017; their micrographs are reproduced as outline drawings in Figs 9–12). Only very few scientists, including Hoppenrath (2004) and Elbrächter and Hoppenrath (in Hoppenrath *et al.*, 2009), rejected Dodge's interpretations.

Clarification of this confusing situation is only possible by a thorough re-investigation of the taxon originally described by Schiller. No original physical material is available and thus, samples collected at the type locality in Trieste were used to establish clonal strains of planktonic cells assigned to *Prorocentrum*. One strain corresponding to Schiller's original drawing of *P. triestinum* is used for epitypification. Strains identified as *P. redfieldii* from the north-eastern Atlantic and from the Mediterranean are also examined for morphological and phylogenetic comparison.

Materials and methods

Sampling, cell isolation and cultivation

Strain 1069 determined as *Prorocentrum triestinum* was isolated from a sample collected at the small Trieste harbour of Santa Croce (45°43.56'N, 13°41.40'E; salinity 35.5, temperature 25.2°C, 19 Sep 2018). Strains 1032 and 1033 determined as *Prorocentrum redfieldii* were isolated from net samples collected at site C1 (45°42.050'N, 13°42.767'E; isolated on 19 Jan 2014) and site Acegas (45°38.605'N, 13°40.861'E; isolated on 21 Jan 2014), both located in the Adriatic Sea in the Gulf of Trieste. Single cells were transferred into single wells of 24-well tissue culture plates (Corning; New York, New York, USA) containing 1 ml of medium B (Agatha *et al.*, 2004) diluted 1:3 with filtered seawater using drawn micropipettes under an SZX10 dissection microscope (Olympus; Hamburg, Germany). Isolates were incubated at 15°C under low light (50 µmol photons m^{-2} s^{-1}) at a light:dark cycle of 12:12 hours. Finally, cultures were adapted to full strength medium B and kept in the culture collection CoSMi at the Instituto Nazionale di Oceanographia e di Geophisica Sperimentale (OGS), Trieste.

Two additional strains of *P. redfieldii* (1-B8 and 1-B9) were established from surface water samples (salinity: 33.34, temperature: 18.9°C) collected in the southern North Sea off Belgium at 51°30.50'N, 2° 40.88'E. Single cells were isolated by micropipetting under a stereomicroscope M5A (Wild; Heerbrugg, Switzerland) and transferred into individual wells of 96-well tissue culture plates (TPP; Trasadingen, Switzerland) each containing 250 µl of K-medium (Keller *et al.*, 1987) prepared from 0.2 µm sterile-filtered natural Antarctic seawater diluted 1:10 with filtered seawater from the sampling location. Plates were incubated at 15°C under low light (30 µmol photons m^{-2} s^{-1}) in a controlled environment growth

chamber (Model MIR 252, Sanyo Biomedical; Wood Dale, Illinois, USA). After 3–4 weeks, both strains were inoculated into 65 ml polystyrene cell culture flasks. Growth medium was enriched with nutrients corresponding to 50% of K-medium.

For DNA harvest, cells were collected by centrifugation (model 5810R, Eppendorf; Hamburg, Germany) in 50 ml centrifugation tubes at 3 220×*g* for 10 min. Cell pellets were transferred to 1 ml microtubes, then centrifuged again (model 5415, Eppendorf, 16 000×*g*, 5 min) and stored frozen (−20°C) for subsequent DNA extraction.

Microscopy

Observation of living or fixed cells (formaldehyde: 1% final concentration, or neutral Lugol-fixed: 1% final concentration) by light microscopy (LM) was carried out using an inverted (Axiovert 200M, Zeiss; Jena, Germany) and a compound microscope (Axiovert 2, Zeiss), both equipped with epifluorescence and differential interference contrast optics. The shape and location of the nucleus was determined after staining of formalin-fixed (1% final concentration) cells with 4',6-diamidino-2-phenylindole (DAPI, 0.1 µg ml^{-1} final concentration) for 10 min. Images were taken either with a digital camera (Axiocam MRc5, Zeiss), or videos were recorded using a digital camera (Gryphax Jenoptik; Jena, Germany) at full-HD resolution. Single frame micrographs were then extracted using Corel Video Studio software (Version X8, Coral; Ottawa, Canada).

Cell length and depth of freshly neutral Lugol fixed cells (1% final concentration) from dense but healthy and growing strains (based on stereomicroscopic inspection of the living material) during late exponential phase were measured at microscopic magnification of 640× using the inverted microscope and the Axiovision software (Zeiss).

For scanning electron microscopy (SEM), cells were collected by centrifugation (model 5810R, Eppendorf, 3220×*g* for 10 min) from 15 ml of culture. The supernatant was removed and the cell pellet resuspended in 60% ethanol prepared in a 2 ml microtube with seawater (final salinity ~13) at 4°C for 1 h in order to strip off the outer cell membrane. Cells were further collected by centrifugation (model 5415R, Eppendorf, 16 000×*g* for 5 min) and resuspended and fixed in a 60:40 mixture of deionised water and seawater (final salinity ~13) with the addition of formaldehyde (1% final concentration) and stored at 4°C for 3 h. Cells were collected on polycarbonate filters (25 mm Ø, 3 µm pore-size, Millipore Merck; Darmstadt, Germany) in a filter funnel, in which all subsequent washing and dehydration steps were carried out. A total of eight washing steps (2 ml MilliQ-deionised water each) were followed by a dehydration series in ethanol (30%, 50%, 70%, 80%, 95%, 100%; 10 min each). Filters were chemically dried with hexamethyldisilazane (HMDS), first in 1:1 HMDS:EtOH, followed by 100% HMDS twice and then stored in a desiccator under gentle vacuum. Finally, filters were mounted on stubs, sputter coated (Emscope SC500; Ashford, UK) with gold-palladium and viewed at 10 kV under a SEM (FEI Quanta FEG 200; Eindhoven, the Netherlands). Micrographs were presented on a black background using Photoshop 6.0 (Adobe Systems; San Jose, California, USA).

DNA extraction and sequencing

Genomic DNA was extracted from fresh material of strains 1069, 1032, 1033 and 1-B8 according to the manufacturers' instructions (NucleoSpin Soil Kit, Machery-Nagel, Düren, Germany) with the following adjustment: The bead tubes were shaken (not vortexed) for 45 s and another 30 s at a speed of 4.0 m s^{-1} in a cell disrupter (FastPrep FP120, Thermo-Savant, Illkirch, France). DNA was stored at −20°C until further processing.

Various regions of the ribosomal RNA (rRNA) genes including the small subunit (SSU/18S), both internal transcribed spacers (ITS) and the D1/D2 region of the large subunit (LSU/28S) were amplified using the following primer pairs: 1F (5′-AAC CTG GTT GAT CCT GCC AGT-3′) and 1528R (5′-TGA TCC TTC TGC AGG TTC ACC TAC-3′) for SSU (Medlin *et al.*, 1988); ITSa (5′-CCA AGC TTC TAG ATC GTA ACA AGG (ACT)TC CGT AGG T-3′) and ITSb (5′-CCT GCA GTC GAC A(GT)A TGC TTA A(AG)T TCA GC(AG) GG-3′) for ITS (Adachi *et al.*, 1996); DirF (5′-ACC CGC TGA ATT TAA GCA TA-3′) and D2CR (5′-CCT TGG TCC GTG TTT CAA GA-3′) for LSU (Scholin *et al.*, 1994).

Each 20 µl PCR reaction contained 16.3 µl of ultrapure H_2O, 2.0 µl of HotMaster Taq buffer (5Prime; Hamburg, Germany), 0.2 µl of each primer (10 µM), 0.2 µl of dNTPs (10 µM), 0.1 µl of Taq Polymerase (Quantabio; Beverly, Massachusetts, USA) and 1.0 µl of extracted DNA template (10 ng $µl^{-1}$). Then, PCR were conducted in a Nexus Gradient Mastercycler (Eppendorf) with the following conditions:

SSU amplification was performed by initialisation at 94°C for 5 min; 30 cycles of 94°C for 2 min, 55°C for 2 min, 68°C for 3 min and a final extension at 68°C for 10 min. For ITS amplification, the settings were: 94°C for 4 min, followed by 10 cycles at 94°C for 50 s, 58°C for 40 s, 70°C for 1 min and then 30 cycles at 94°C for 45 s, at 50°C for 45 s, at 70°C for 1 min and a final extension at 70°C for 5 min. The D1/D2 region (LSU) was amplified by initialisation at 94°C for 2 min, followed by 30 cycles at 94°C for 30 s, at 55°C for 30 s, at 65°C for 2 min and a final extension at 65°C for 10 min. To verify the expected amplicon lengths, the PCR products were

checked on a 1% agarose gel (in TE buffer, 70 mV, 30 min). The PCR amplicons were purified using the NucleoSpin Gel and PCR clean-up kit (Macherey-Nagel) and sequenced directly in both directions on an ABI PRISM 3730XL (Applied Biosystems by Thermofisher Scientific; Waltham, Massachusetts, USA) as described in Tillmann *et al.* (2017). Raw sequence data were processed using the CLC Genomics Workbench 12 (Qiagen; Hilden, Germany).

Molecular phylogenetics

A systematically representative set of prorocentralean accessions was compiled from known dinophyte reference trees such as presented in Gottschling *et al.* (2020). The sample was enriched by all those sequences deposited in GenBank, which showed ultimately close relationships to the sequence data gained in the present study, as inferred from BLAST searches (Altschul *et al.*, 1990). Voucher information is provided in Supplementary table S1, which also includes outgroup details comprising dinophytes of the Dinophysales and Gymnodiniales.

For alignment, separate matrices of the rRNA operon (i.e. SSU, ITS, LSU) were constructed, aligned using 'MAFFT' v6.502a (Katoh & Standley, 2013) and then concatenated. The aligned matrices are available as triestinum.nexus file in the Supplementary Information. Phylogenetic analyses were carried out using maximum likelihood (ML) and Bayesian approaches, as described previously (Gottschling *et al.*, 2020) using the resources available from the CIPRES Science Gateway (Miller *et al.*, 2010). The Bayesian analysis was performed using MrBayes v3.2.6 (Ronquist *et al.*, 2012, freely available at http://mrbayes.sorceforge.net/download.php) under the GTR+Γ substitution model and the random-addition-sequence method with 10 replicates. Two independent analyses of four chains (one cold and three heated) with 20 000 000 generations were run, sampled every 1000th cycle, with an appropriate burn-in (10%) as inferred from the evaluation of the trace files using Tracer v1.5 (http://tree.bio.ed.ac.uk/softw are/ tracer/). For the ML calculation, the MPI version of RAxML v8.2.4 (Stamatakis, 2014, freely available at http://www.exelixislab.org/) was applied using the GTR+Γ substitution model under the CAT approximation. We determined the best-scoring ML tree and performed 1000 non-parametric bootstrap replicates (rapid analysis) in a single step. Statistical support values (LBS: ML bootstrap support, BPP: Bayesian posterior probabilities) were drawn on the resulting, best-scoring tree.

Terminology

Terminology of cell orientation, designation of thecal plates and platelets and ornamentation follows Hoppenrath *et al.* (2013) supplemented by Tillmann *et al.* (2019).

Results

Morphology

Prorocentrum triestinum

Cells of strain 1069 were asymmetric in outline (Figs 13–22). In lateral view, the ventral curvature was narrowly obovate, whereas the dorsal curvature was elliptic, with cells having their largest depth in the median. Cellular asymmetry was accentuated by the dorso-subapical position of a small spine (Figs 13–21). In ventral and dorsal views, cell shape was slightly asymmetric as well, with the outline of the left thecal plate being slightly wider compared with the right thecal plate (Figs 16, 22). In lateral view, the posterior end was acute (Figs 13, 17, 20, 21). In older cells, for example those with broad growth bands, the posterior end was truncate in dorsal or ventral view (Figs 16, 22). Cell size ranged from 20.1–25.8 µm in length and 10.9–15.6 µm in depth (Table 1). Fixed cells rarely settle in dorsal/ventral view and subsequently, cell width was more difficult to measure. Based on LM measurements of five cells in ventral/dorsal view cell width ranged from 10.6–18.3 µm.

Cells were yellow-brown in colour (Figs 13–18) and included two reticulate chloroplasts (Fig. 24), which were parietally arranged with respect to each of the large thecal plates. A number of long (up to 7 µm), rod-shaped structures (probably trichocysts) in the anterior part of the cells were arranged along (Fig. 17), or at a slightly acute angle with respect to, the cell's longitudinal axis (Fig. 18). On empty thecae, the main area of thecal plates was smooth, whereas a few pores were visible, usually close to the sagittal suture (Fig. 23). A large and globose or slightly ovoid nucleus was located in the posterior part of the cell (Fig. 25), which was more elongated in ventral view during cell division (Figs 26, 27). The pusule, a hyaline organelle of varying size, was occasionally visible in the anterior part of the cell (Figs 16, 18).

Scanning electron microscopy confirmed the general appearance of the cell and the three-dimensional shape of both thecal plates in more detail (Figs 28–36). In lateral view, both dorsal and ventral sides were convex, with the dorsal side being broader (Figs 28–31). The ventral side, with a slender obovate outline, was longer and had an elevated apical-ventral part (Figs 28, 31). The intercalary band between both plates was variable in width and only faintly striated horizontally (Figs 34–36, 42, 43). The anterior spine was broad in ventral view, roughly as broad as the spine was tall (Figs 35, 36). Total length of the spine was 1.5 ± 0.2 µm (min 1.1 µm, max 1.9 µm) (Table 1).

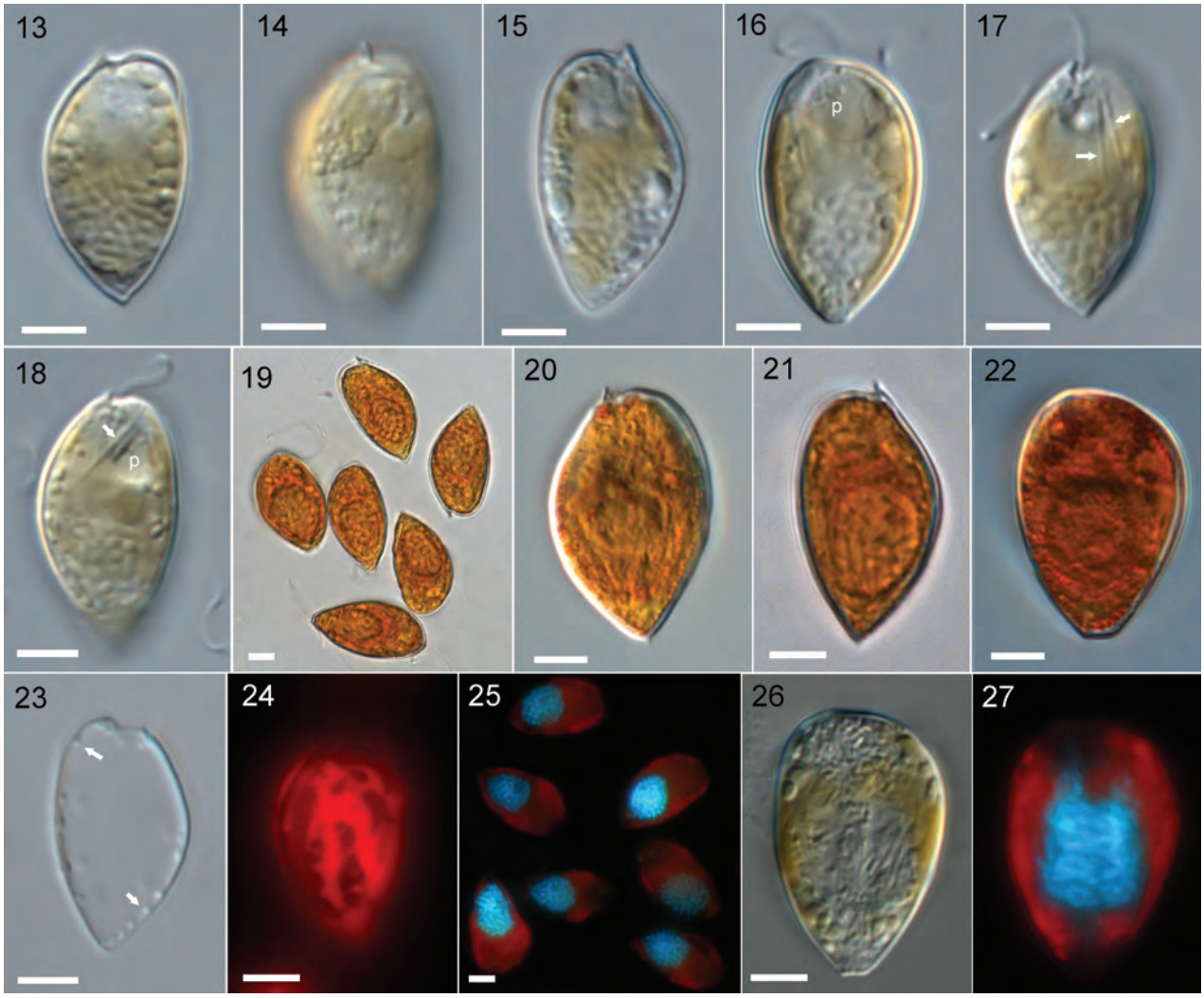

Figs 13–27. *Prorocentrum triestinum* (strain 1069) LM. **Figs 13–18**. Living cells. **Figs 19–22**. Lugol-fixed cells. **Figs 24–27**. Formaldehyde-fixed cells. **Figs 13–22**. General size and shape of cells in lateral view of the right thecal plate (Figs 13, 14, 17, 18, 20), the left thecal plate (Figs 15, 21) and in ventral view (Figs 16, 22). Note the large apical trichocyst rods (arrows in Figs 17, 18), the thick chromosomes visible in Figs 13, 16, 17, 18, the presence of thecal pores (arrow) visible on the empty theca in Fig. 23 and the presumptive pusule (p) in Figs 16, 18. **Fig. 24**. Cell in epifluorescence and blue light excitation to illustrate chloroplasts' shape and distribution. **Fig. 25**. Cells stained with DAPI with UV excitation to illustrate shape and position of the nucleus. **Figs 26, 27**. The same cell stained with DAPI in brightfield (Fig. 26) and with UV excitation (Fig. 27) to illustrate shape and position of the nucleus during nuclear division. Scale bars: 5 μm.

Thecal plates were smooth and had a few pores of three different types (Figs 37–43). The first type was characterised by large pores, each with a tubular structure counter-sunk into a depression (Figs 37, 38, 41, 42). The diameter of the pores and the pore openings averaged 0.46 ± 0.05 μm and 0.17 ± 0.02 μm, respectively (Table 2). The internal tubular structure of large trichocyst pores was discernible (Figs 39, 40). The second type was characterised by small pores (Figs 37, 38, 40, 41: black arrows), which were not counter-sunk and had slightly smaller diameters (0.14 ± 0.01 μm; Table 2). Internal thecal views revealed that the small pores had a distinctly smaller inner extension compared with large pores (Fig. 40). The third type was characterised by an occasional single mini-pore at the posterior end of a thecal plate (Fig. 41: white arrow); the diameter of these pores was even smaller (0.07–0.08 μm; Table 2).

The number of large and small trichocyst pores was roughly the same on both lateral plates and was about 17 and 6 for each plate, respectively (Figs 28–31, Table 2). Position of thecal pores varied slightly. A row of a few (usually 5) large pores was typically accompanied by a few small pores (usually 2) in apical position on the right thecal plate (Figs 28, 29, 44). Rows of pores (mostly 3–5 large pores) were also present on the posterior dorsal side of both plates (Figs 35–37, 42) and thus visible in dorsal but not ventral view. A few pores, roughly arranged in two rows running perpendicular to the cell's longitudinal axis, were also present (Figs 28, 29).

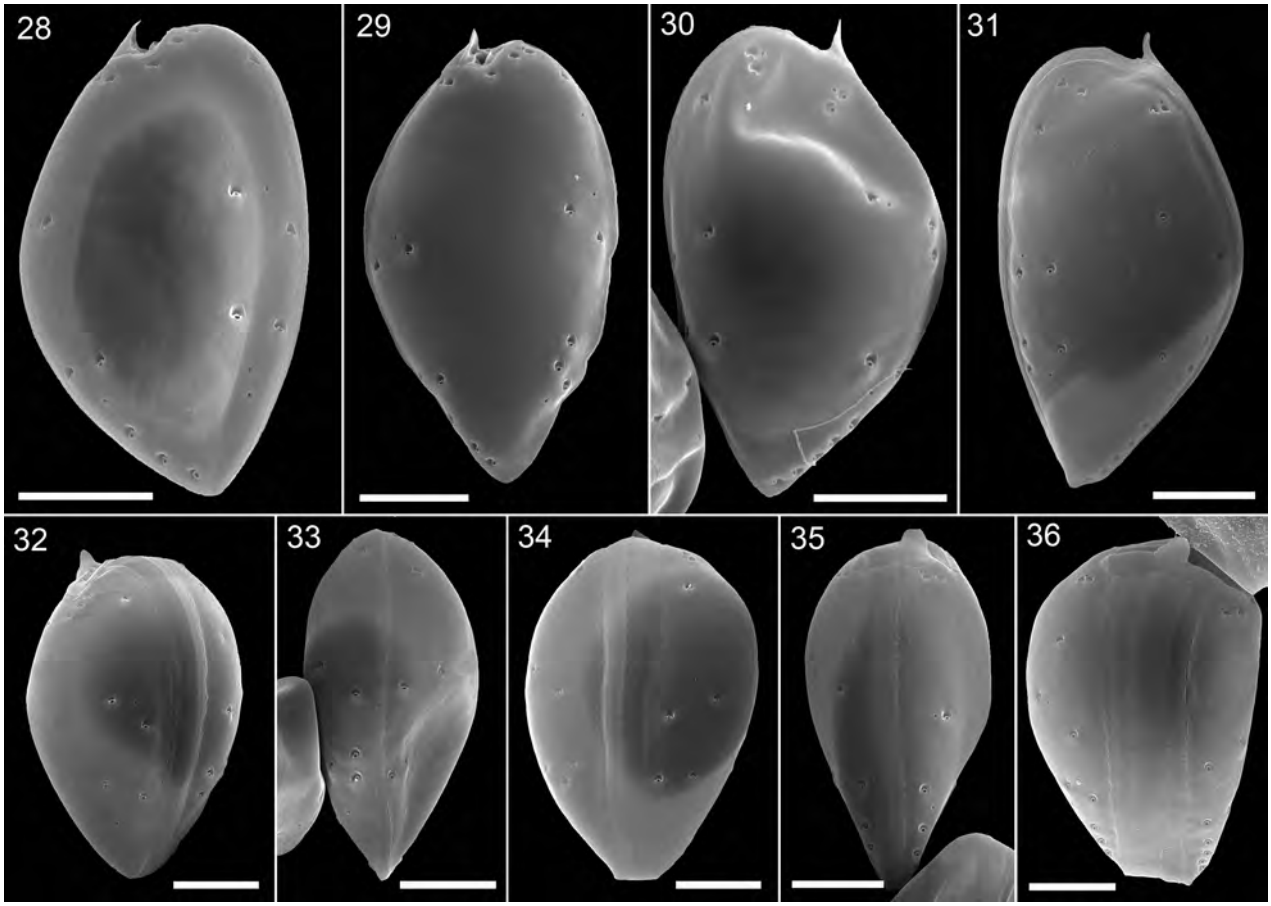

Figs 28–36. *Prorocentrum triestinum* (strain 1069) SEM, entire cells. **Figs 28, 29**. Cells in right thecal view. **Figs 30, 31**. Cells in left thecal view. **Fig. 32**. Cell in ventral-right lateral view. **Figs 33, 34**. Cells in ventral view. **Figs 35, 36**. Cells in dorsal view. Scale bars: 5 µm.

Table 1. Size of cells and of the apical spine for *Prorocentrum triestinum* and *P. redfieldii* strains (length, depth: LM; spine: SEM).

		Length (µm)	Depth (µm)	l/d ratio		Spine length (µm)	
Species	Strain	Mean ± SD min – max	Mean ± SD min – max	Mean ± SD	n	Mean ± SD min – max	n
P. triestinum	1069	22.3 ± 1.2 20.1 – 25.8	12.7 ± 1.1 10.9 – 15.6	1.76 ± 0.11	75	1.5 ± 0.2 1.1 – 1.9	40
P. redfieldii	1032	32.6 ± 1.2 29.5 – 36.1	10.7 ± 1.1 8.5 – 13.1	3.08 ± 0.26	42	5.6 ± 0.6 4.1 – 6.4	32
P. redfieldii	1033	32.1 ± 1.3 27.9 – 34.2	10.6 ± 1.2 8.5 – 13.2	3.05 ± 0.33	43	5.5 ± 0.6 3.4 – 6.7	40
P. redfieldii	1-B8	24.9 ± 1.6 21.8 – 29.7	9.4 ± 1.3 7.2 – 14.0	2.69 ± 0.28	120	4.2 ± 0.6 3.2 – 5.9	35
P. redfieldii	1-B9	26.6 ± 1.5 23.7 – 30.4	9.4 ± 1.2 9.9 – 11.5	2.85 ± 0.31	89	4.4 ± 0.6 3.1 – 5.6	38

The dorso-subapical positioned periflagellar area (Figs 44–52) was ~3.2 µm deep and 2.3 µm wide. It was located in a small V- to U-shaped indentation of the right thecal plate (Figs 29, 44, 51, 52) and composed of eight platelets (Figs 46–52). There was a relatively large, irregularly ovate flagellar pore (fp), which was longer than wide. The fp was surrounded by platelets 3, 5, 6 and 8, all of which bore low lists bordering the fp (Figs 47–52). The fp was closed by two lip-like structures (Figs 48–50). A minute accessory pore (ap) was located dorsally from the flagellar pore, between platelet 8 and a relatively small, narrow, elongated platelet 7 (Figs 47, 49–52). The triangular platelet 1 was the largest of the periflagellar platelets and had the apical spine (Figs 44, 47–49) which was wider than long, wing-like, but distally acute (Figs 44, 45, 49, 50). Platelet 2 was small and smooth and had no list (Figs 49–52). Platelet 3 had a deeper cavity (Figs 47, 48, 50) and occasionally ally with a pore (Fig. 46). The irregularly quadrangular and plain platelet 4 was opposite platelet 1 (Figs 48, 50, 52). Platelet 5 was J-shaped and platelet 6 elongated (Figs 47–52).

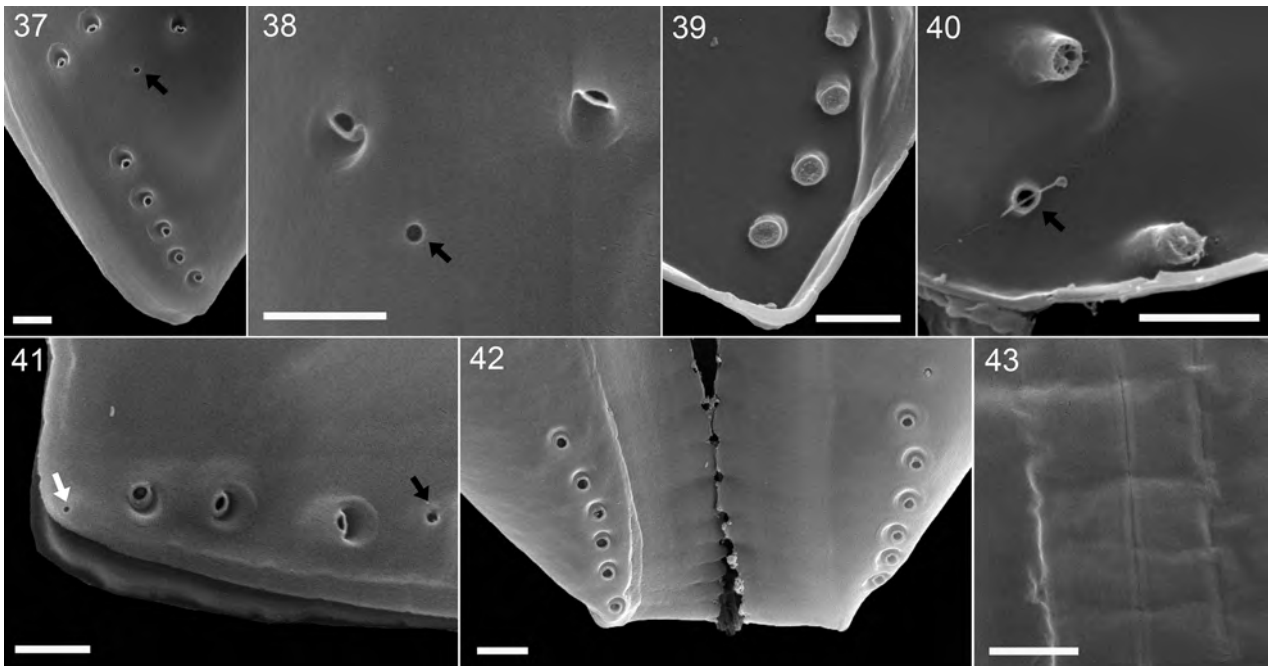

Figs 37–43. *Prorocentrum triestinum* (strain 1069), detailed SEM of surface structure and pores. **Fig. 37**. Posterior end of the right thecal plate showing large tubular pores and a small thecal pore (black arrow). **Fig. 38**. Detailed view of large and small (black arrow) pores. **Figs 39, 40**. Internal view of large and small (black arrow) pores. **Fig. 41**. Posterior end of the left thecal plate illustrating a mini-pore located at the most posterior tip of the thecal plate (white arrow), which is distinctly smaller that the small pore (black arrow). **Figs 42, 43**. Detailed view of the intercalary band with faint horizontal striae and a few transverse furrows. Scale bars: 1 μm.

Prorocentrum redfieldii

All four strains of *P. redfieldii* were morphologically identical when examined by LM and SEM. Cells were slender (Figs 53–61, Supplementary figs S1–S12), with a length/depth ratio of 2.69 (strain 1-B8) to 3.08 (strain 1032) (Table 1). The anterior end was rounded and had a long and prominent apical spine. The posterior end was acute in lateral views (Figs 56, 62–65, Supplementary figs S1, S13, S14). In ventral or dorsal view, it was acute in slender cells (Figs 58, 59) but truncated in wide (presumably old) cells (Figs 60, 66, 68, Supplementary figs S15–S17). Occasionally, the posterior end had a minute, drop-shaped extension (Fig 62, Supplementary figs S2, S3). Cell size for all strains ranged from 21.8–36.1 μm in length and 7.2–14.0 μm in depth (Table 1). Both Mediterranean strains were slightly but significantly larger than both North Sea strains (Student's t-test: $t = 30.2$, $p < 0.001$).

A few very long (~10 μm) rod-shaped structures (presumably trichocysts) were visible in the anterior part of the cells (Fig. 55, Supplementary figs S1, S7). Two parietally arranged reticulate chloroplasts (Fig. 61, Supplementary fig. S11) of yellowish-brown colour (Figs 54–56, 58–60, Supplementary figs S1–S9) were present. The pusule, a hyaline organelle of varying size, was occasionally visible in the anterior part of the cell (Fig. 59, Supplementary fig. S8). Plates of empty thecae were smooth with a few pores mainly located close to the sagittal suture (Fig. 57, Supplementary fig. S10). A large, ovoid nucleus was located in the posterior part of the cell (Fig. 61, Supplementary fig. S12).

Scanning electron microscopy revealed the three-dimensional shape of cells in more detail (Figs 62–69, Supplementary figs S13–S20). The dorsal and ventral sides of both plates were slightly convex (Figs 62–65, Supplementary figs S13, S14). Cells with a broad growth band were almost as wide as deep in dorsal or ventral view (Fig. 66, Supplementary figs S16, S17). In lateral view, cells were almost symmetrical, although the dorsal convexity was slightly wider (Figs 62–65, Supplementary figs S13, S14). The spine was long (3.1–6.7 μm, Table 1) and slender in lateral view (Figs 62–65, Supplementary figs S13, S14) and was slightly but significantly longer for both Mediterranean strains compared with those from the North Sea (Student's t-test: $t = 12.6$, $p < 0.001$). The spine was triangular with a broader base in dorsal or ventral view (Figs 66, 68, 69, Supplementary figs S16, S19, S20). The intercalary band between both thecal plates was of varying width (Figs 66, 68, 69, Supplementary figs S15–S20) with faint and variable horizontal striations (Fig. 70, Supplementary fig. S15).

Thecal plates were smooth with a few pores of three different types (Figs 70–73, Supplementary figs S21, S22). The majority of pores were large, tubular, and located in larger depressions. Pore and depression diameters ranged from 0.13–0.23 μm and 0.41–0.70 μm, respectively (Table 2). Pores of

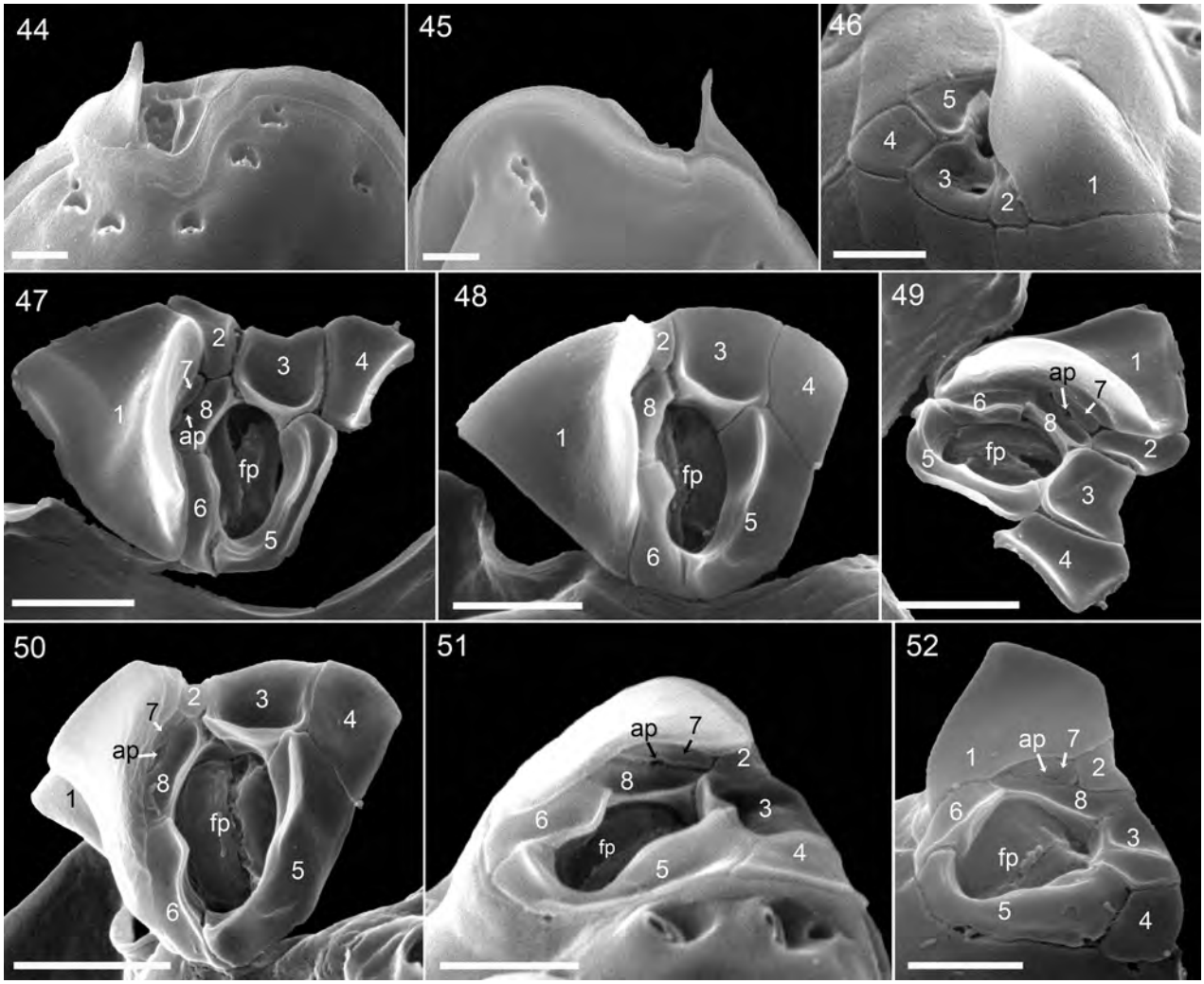

Figs 44–52. *Prorocentrum triestinum* (strain 1069), detailed SEM of the periflagellar area. **Fig. 44**. Right lateral to apical view. **Fig. 45**. Left lateral view. **Fig. 46**. Apical left lateral view of the periflagellar area. **Figs 47–52**. Various apical views of detached periflagellar areas of different cells showing the detailed arrangement of periflagellar platelets and platelet variability (Fig. 52, note that here platelet 8 exceptionally separates platelet 2 and 3). ap, accessory pore; fp, flagellar pore. Scale bars: 1 μm.

the second type were simple, small holes in the theca with diameters ranging from 0.14–0.18 μm (Table 2). A single mini-pore (type 3; 0.07–0.10 μm; Table 2; Supplementary fig. S21) was occasionally present at the posterior tip of the theca, which was slightly smaller in diameter than the other small pores. The number of pores per plate was variable (Table 2). Large pores were three to four times more abundant than small pores and present in roughly equal numbers on both thecal plates. Mediterranean strains had slightly more pores compared with North Sea strains (Table 2). Large (trichocyst) pores formed characteristic patterns in the apical area (Figs 62–69, Supplementary figs S13–S20). While a curved row of approximately five large pores and two small pores was present on the right thecal plate (Figs 62, 63, 74, Supplementary fig. S13), four pores were typically present in a more scattered position on the left thecal plate (Figs 64, 65, Supplementary fig. S14). Conspicuous rows of three to seven pores were present on the posterior dorsal sides of both plates (Fig. 68, Supplementary figs S18–S20). Pores in the middle of the thecal plates were more scattered in two to three indistinct rows running perpendicular to the cell's longitudinal axis (Figs 62–65, Supplementary figs S13, S14).

The periflagellar area was composed of eight platelets (Figs 74–78, Supplementary fig. S24). Platelets 3, 5, 6 and 8 surrounded a large and irregularly oval flagellar pore, which was closed by two lip-like structures. A minute accessory pore was between platelets 7 and 8. Platelet 1 was the largest and had the long apical spine (Figs 74, 77, Supplementary fig. S23). Platelet 4 was plain, whereas very low lists were present on the platelets surrounding the flagellar pore. Platelet 5 was J-shaped and platelet 6 elongated.

Table 2. Number and size of pores for *Prorocentrum triestinum* and *P. redfieldii* strains. Data are listed as mean ± SD (first row) and min–max (second row). n = number of observations. Mini-pore diameter statistics are based on combined measurements of strains 1033 and 1-B8. n.d. = not determined.

		Number of pores per thecal plate						Pore size					
		Right thecal plate			Left thecal plate			Large pores			Small pores		
Species	Strain	Large	Small	n	Large	Small	n	Outer Ø µm	pore Ø µm	n	Ø µm	n	Mini-pores Ø µm	n
P. triestinum	1069	17.3 ± 1.7	5.8 ± 0.9	29	17.1 ± 2.0	5.4 ± 0.6	27	0.46 ± 0.05	0.17 ± 0.02	20	0.14 ± 0.01	20	0.07 ± 0.01	7
		13–21	5–9		12–20	4–6		0.36–0.58	0.12–0.21		0.11–0.15		0.07–0.08	
P. redfieldii	1032	21.0 ± 1.8	5.6 ± 0.7	22	18.5 ± 2.2	5.5 ± 0.7	22	n.d.	n.d.		n.d		n.d	
		18–24	4–7		15–23	4–7								
P. redfieldii	1033	20.7 ± 2.3	5.3 ± 0.6	20	18.9 ± 1.5	5.1 ± 0.8	21	0.55 ± 0.07	0.18 ± 0.02	22	0.15 ± 0.01	20	0.08 ± 0.01	10
		16–26	4–6		16–22	4–7		0.41–0.70	0.13–0.23		0.14–0.18		0.07–0.10	
P. redfieldii	1-B8	18.3 ± 3.6	5.4 ± 0.7	20	15.3 ± 2.1	4.8 ± 0.9	20	0.47 ± 0.04	0.16 ± 0.01	20	0.15 ± 0.01	20		
		12–24	4–7		12–19	3–6		0.41–0.58	0.14–0.19		0.14–0.17			
P. redfieldii	1-B9	17.0 ± 3.4	5.4 ± 1.0	21	16.1 ± 3.3	5.0 ± 0.8	20	n.d	n.d		n.d		n.d	
		11–23	4–7		10–22	4–6								

Molecular phylogenetics

The SSU+ITS+LSU alignment was 1789+745+3473 bp long and composed of 288+522+825 parsimony-informative sites (27%, mean of 19.94 per terminal taxon) and 2 657 distinct RAxML alignment patterns. Figure 79 shows the best-scoring ML tree (–ln = 52 177.36; being highly similar to the Bayesian tree), with the internal topology not fully resolved. Three lineages, respectively including *Adenoides* Balech (100LBS, 1.00BPP), *Plagiodinium* R.D.Saunders & J.D. Dodge (100LBS, 1.00BPP) and *Prorocentrum*, formed a well-supported clade (80LBS, 1.00BPP). *Prorocentrum* segregated into two clades, denominated here PRO1 including the type *P. micans* (100LBS, 1.00BPP) and PRO2 (97LBS, 1.00BPP). PRO1 consisted of three clades, one of which was comprised of benthic species such as *P. emarginatum* Fukuyo (96LBS, 1.00BPP), and the second constituted the *P. micans* species complex (64LBS, 0.98BPP). The third clade (93LBS, 1.00BPP) included all accessions of the two species under study here, together with *P. obtusidens* and *P. cordatum* (100LBS, 1.00BPP). As inferred from short branches, sequence divergence was distinct but low between *P. triestinum* (single accession) and *P. redfieldii* (96LBS, 0.99BPP), and both constituted sister species (100LBS, 1.00BPP). The primary sequence of *P. triestinum* differed from those assigned to *P. redfieldii* at four alignment positions in the SSU, seven in the ITS region and two in the LSU.

Discussion

Prorocentrum triestinum *isolated from the type locality*

Clonal strain 1069, isolated from the type locality (Trieste) and documented here in detail, corresponds to the protologue and the original drawings of *P. triestinum* (Fig. 1; Schiller, 1918). However, Schiller's description of his new species has to be treated with caution, as he claimed that one of the lateral plates ('Schale') was acute ('spitz') posteriorly, whereas the other plate was bluntly truncate ('stumpf abgeschnitten'). This wording may seem to contradict our description, but it precisely corresponds to the taxon observed here, assuming that his description of the right side was in fact a misinterpretation of the dorsal view of older cells with wide growth bands, where the posterior cell end is truncate and ends straight (see Figs 22, 26). Schiller's descriptions of *P. triestinum* varied over time (Schiller, 1918, 1928, 1933), because there were not yet any established concepts of cell orientation and morphological terminology. As discussed in Hoppenrath *et al.* (2013), this complicates interpretation of early descriptions. For example, Schiller described the anterior spine as solid ('solider Stachel') having no recognisable wing

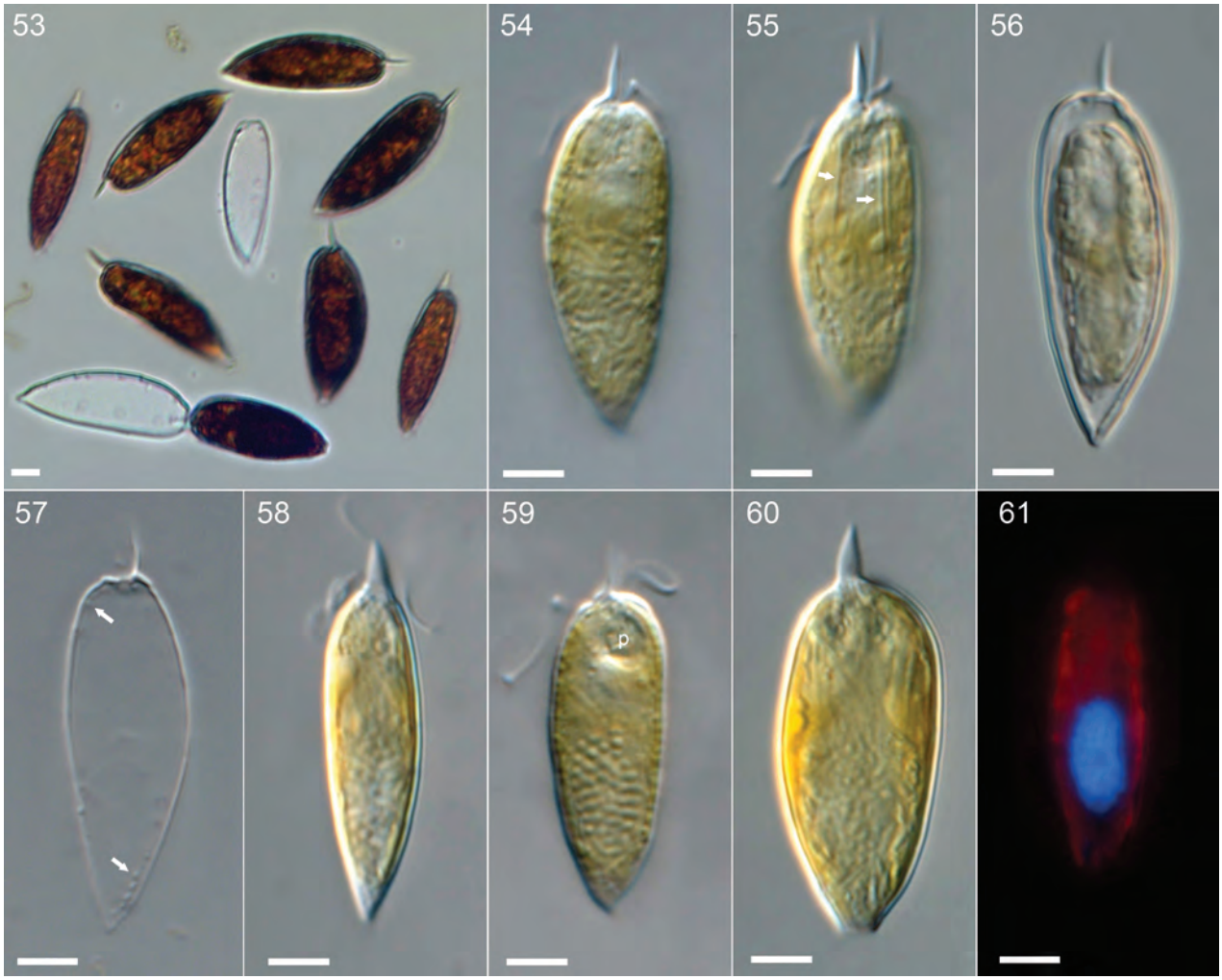

Figures 53–61.: *Prorocentrum redfieldii* (strain 1-B8) LM. **Fig. 53**. Lugol-fixed cells. **Figs 54, 55, 58–60**. Living cells. **Figs 56, 61**. Formaldehyde-fixed cell. **Figs 53–60**. General size and shape of cells in lateral view of the right thecal plate (Figs 54, 55), of the left thecal plate (Figs 56, 57) or in dorsal (Fig. 58) and ventral view (Fig. 60). Note the long apical trichocyst rods (arrows in Fig. 55), the thick chromosomes visible in Figs 54, 59, the presence of thecal pores (arrows) visible on the empty theca in Fig. 57 and the presumptive pusule (p) in Fig. 59. **Fig. 61**. Cell stained with DAPI with UV excitation to illustrate shape and position of the nucleus. Scale bars: 5 μm.

(Schiller, 1918, p. 252) or as a solid tooth ('solider Zahn') with a small wing dorsally located relative to the flagella gap ('Geißelspalt') (Schiller, 1928) or as solid, small thornlet ('solides Dörnchen') with hardly visible wing ventrally located relative to the flagellar gap (Schiller, 1933). Careful inspection of Schillers' drawings is thus necessary and after having done so, we are confident that our collection from the type locality is equivalent to the *P. triestinum* discovered 100 years ago.

We failed to detect *P. triestinum* in the old boat harbour sampled by Schiller (1918), but we were able to isolate the species from that of Santa Croce, which is only 10 km farther up the coast. Schiller (1918) attributed the blooms in the harbour of Trieste to high levels of sewage draining into the surrounding area. Preference for highly eutrophic habitats might explain why *P. triestinum* has decreased in abundance now that wastewater treatment is common. Previous Adriatic monitoring recorded *P. triestinum* but not *P. redfieldii* for the area. These reports were based on Dodge (1982) and Cabrini & Strami (2006) as taxonomic reference which only consider *P. triestinum* (with *P. redfieldii* in synonymy). Thus, the '*P. triestinum*' monitoring counts also include true *P. redfieldii*. Retrospectively, cells corresponding to the true *P. triestinum* have been identified in plankton samples from monitoring station C1 of Trieste, but always in low abundance (D. Fornasaro, personal communication).

Prorocentrum triestinum *and* P. redfieldii *are different species but closely related*

With the new strains of *P. triestinum* and *P. redfieldii* at hand, morphological differences clearly indicated in the original descriptions of the two taxa are here confirmed at the species level. Thus, the long-lasting misidentification of *P. redfieldii* as *P. triestinum* can be clarified. The

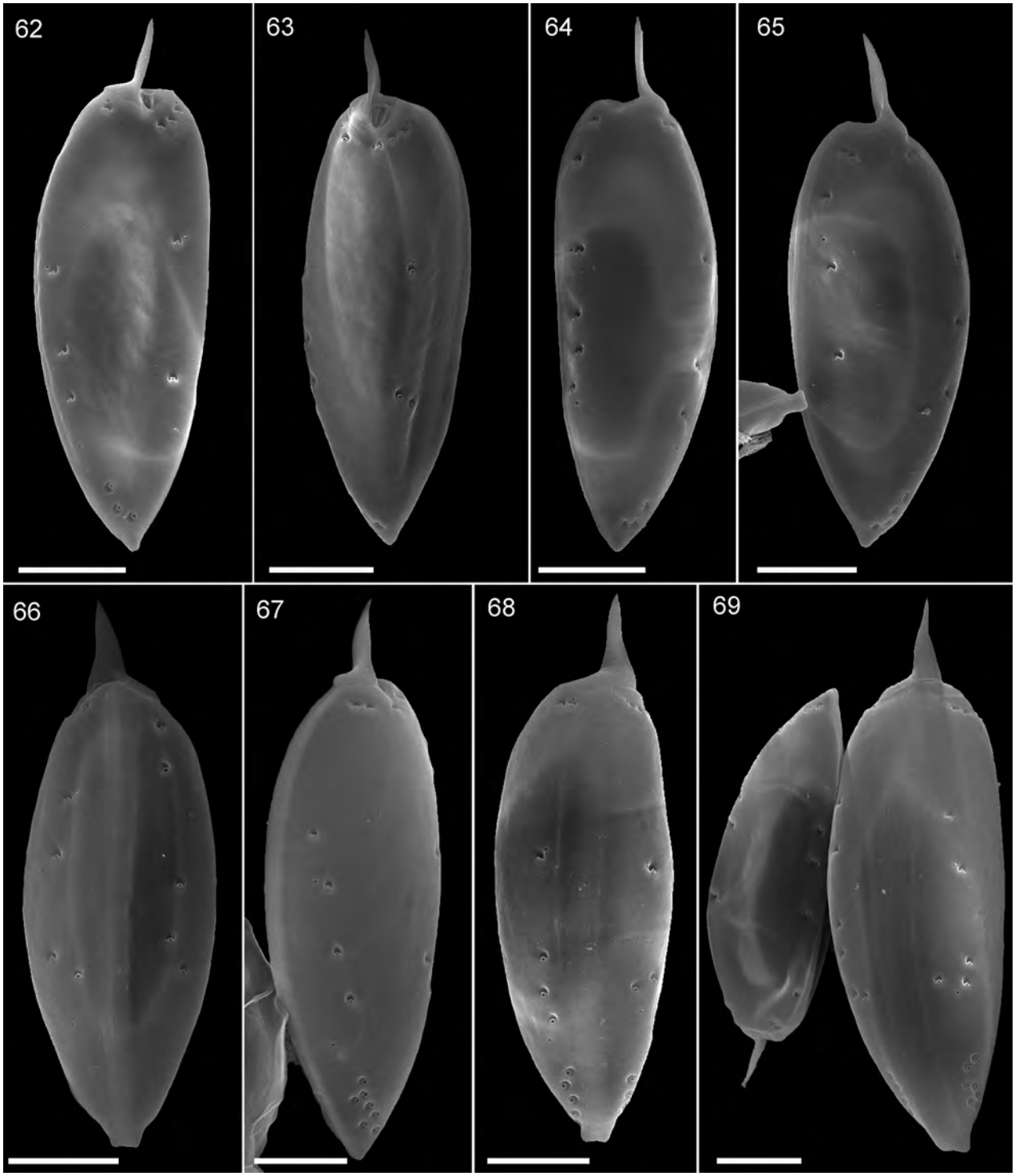

Figs 62–69. *Prorocentrum redfieldii* (strain 1-B8) SEM, entire cells. **Figs 62, 63**. Cells in right lateral view. **Figs 64, 65**. Cells in left lateral view. **Fig. 66**. Cell in ventral view. **Fig. 67**. Cell in right-lateral to dorsal view. **Fig. 68**. Cell in dorsal view. **Fig. 69**. Two cells illustrating differences in cell size. Scale bars: 5 μm.

morphologies of strains are consistent with either *P. triestinum* or *P. redfieldii* and are in agreement with the respective original descriptions (Schiller, 1918; Bursa, 1959). Differences in general cell size, shape and spine morphology allow species delimitation at the LM level. Cells of *P. triestinum*, with their asymmetric outline in lateral view and with a small spine in dorso-subapical position, are remarkably different from the almost symmetric and slender cells of *P. redfieldii* with their longer and apically located spine (Figs 13–22, 53–60, 80–89, Supplementary figs S1–S10). The critical morphometric characters (length/depth ratio and spine length) of the two species did not overlap, notwithstanding some intra-specific morphological variability observed in culture (Table 1). Both species have

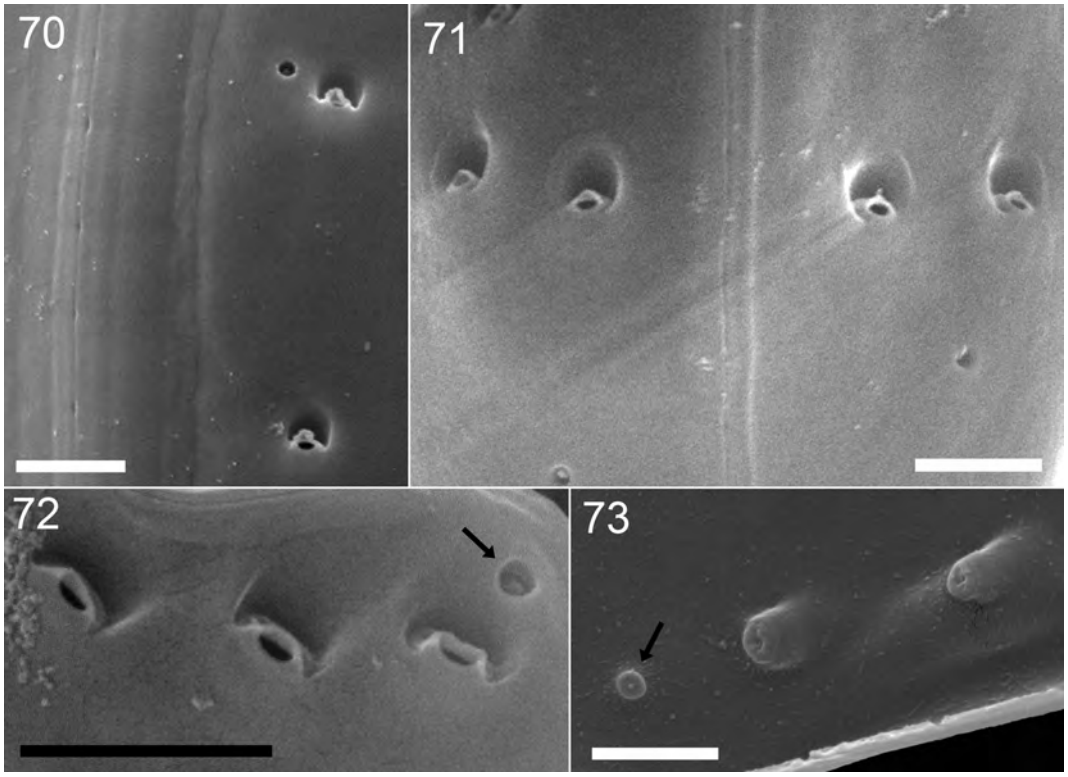

Figs 70–73. *Prorocentrum redfieldii* (strain 1-B8), detailed SEM of surface structure and pores. **Figs 70, 71**. Intercalary band, note the different width and the faint horizontal striae (Fig. 70). **Figs 72, 73**. Large tubular and small pores (black arrow) in external (Fig. 72) and internal (Fig. 73) view. Scale bars: 1 μm.

been found in sympatry in the Trieste region (this study) and in the North Sea (Elbrächter and Hoppenrath in Hoppenrath *et al.*, 2009).

The LSU gene region, and the V4 region of the SSU gene, are the loci commonly used in high-throughput DNA sequencing (HTS) metabarcoding of plankton (Mora *et al.*, 2019; Elfering *et al.*, 2020; Gottschling *et al.*, 2020). Based on our DNA data *P. triestinum* can only be differentiated from *P. redfieldii* using LSU but not SSU sequences, as the four diagnostic positions of the latter are outside the V4 region. The greatest challenge to biological barcoding is the incompleteness of the reference databases and therefore taxonomic, rather than technical in nature (Nilsson *et al.*, 2006; Berney *et al.*, 2017; Gottschling *et al.*, 2020). It will take a long time until unambiguous assignments of morphological and molecular data will enable assessing the entirety of microbial diversity, and our epitypification approach does add reliable data from material equivalent with epitypes. This has particular importance for species described a long time ago such as *Palatinus apiculatus* (Ehrenberg) Craveiro, Calado, Daugbjerg & Moestrup and *P. micans*, of which no reliable DNA was available until their epitypifications (Kretschmann *et al.*, 2018; Tillmann *et al.*, 2019) like in the case of *P. triestinum* reported in the present study.

Despite all morphological differences in cell shape and spine length and position, both *P. triestinum* and *P. redfieldii* are closely related based on molecular sequence data. Moreover, both share a smooth theca and a very similar pore pattern (Figs 80–89, Table 3) with large pores lining the periflagellar depression on the right thecal plate, or with rows of pores posterodorsally on both plates. Most significantly, the periflagellar areas are identical (Figs 84, 89) in terms of number, size and arrangement of platelets. For some but not all cells of *P. triestinum*, a thecal pore is visible on platelet 3, but some cells of *P. redfieldii* may also have such a pore that has not been observed yet. Most importantly, both species share the very conspicuous and largely reduced accessory pore together with a very small platelet 7, and this apomorphy clearly differentiates both species from other species of *Prorocentrum*.

Synonymy and potentially related species

To the best of our knowledge, no literature record of *P. triestinum* conforms with Schiller's original descriptions and drawings. Most current confusion traces back to errors in the revision by Dodge (1975), which led to synonymisation of *P. redfieldii* under *P. triestinum*. It was widely accepted, although Elbrächter and Hoppenrath in Hoppenrath *et al.* (2009) separated the two species, and Throndsen (1983, p. 14) was critical of Dodge's synonymisation. Many authors not only lump *P. triestinum* and *P. redfieldii* together, but also misinterpret morpho-

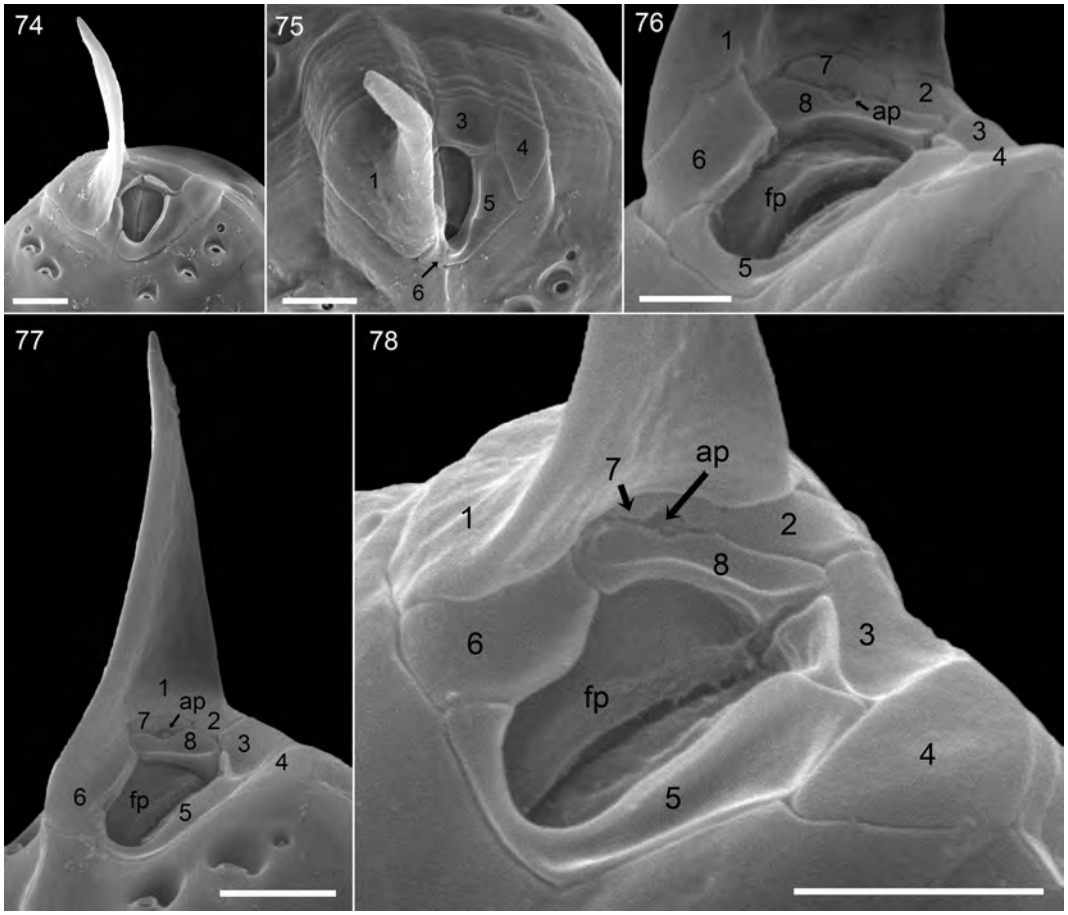

Figs 74–78. *Prorocentrum redfieldii* (strain 1-B8) detailed SEM of the periflagellar area. **Fig. 74**. Apical right-lateral view. **Figs 75–78**. Various views (Fig. 75 apical, Figs 76–78 right ventral apical) of different cells showing the detailed arrangement of periflagellar platelets. ap, accessory pore; fp, flagellar pore. Scale bars: 1 μm.

logical details of true *P. redfieldii*. Loeblich III *et al.* (1979) and Toriumi (1980), for example, overlooked the tiny accessory pore and emphasised the presence of only one anterior flagellar pore. Moreover, Ndhlovu *et al.* (2017) described the tiny accessory pore as part of platelet 8, and also reported a split of platelet 5 in a South African strain of *P. redfieldii* (incorrectly determined as *P. triestinum*). The small platelet 7 (Fig. 89) was also overlooked. Although seeming differences between strains always warrant careful investigation, it is usually possible to correct LM and SEM determinations from (incorrect) *P. triestinum* to (correct) *P. redfieldii* (Adachi, 1972; Loeblich III *et al.*, 1979; Toriumi, 1980; Yoo & Lee, 1986; Okamoto, 1992; Hernández-Becerril *et al.*, 2000; Lu & Goebel, 2001; Ndhlovu *et al.*, 2017).

Other synonymisations are also problematic. Dodge (1975) synonymised *P. pyrenoideum*, a species characterised by the presence of a large pyrenoid and uniquely shaped antapical tubular pores (Bursa, 1959) under his broadly though incorrectly circumscribed *P. triestinum*. *Prorocentrum triestinum* and *P. redfieldii* nevertheless lack these stuctures. Toriumi (1980) considered *P. setoutii* Hada and *P. shikokuense* Hada to be conspecific with *P. redfieldii* (again as *P. triestinum*) on the basis of weak arguments related to similar cell size and identical nucleus shape. *Prorocentrum setoutii* is different from *P. triestinum* by its symmetrically rounded anterior end and the long, 4.0–4.5 μm spine, but its description (Hada, 1975) is inadequate to distinguish it from *P. redfieldii*. Synonymising *P. shikokuense* (recently under *P. obtusidens*, see Shin *et al.*, 2019) with *P. redfieldii* is not acceptable because of its truncate anterior end, missing apical spine, and the thecal ornamentation. For the same reason, it is also dissimilar to *P. triestinum*.

Other records of *P. triestinum* in the literature are for various reasons ambiguous. Böhm (1936) recorded *P. triestinum* from coastal waters of the western Pacific, but his two small drawings show small, slender cells (22–24 μm in length) with a small and central spine and thus correspond neither to *P. triestinum* nor to *P. redfieldii* (Table 3). Dodge (1965), who identified strain L.M. 1136-2 from Plymouth as *P. triestinum*, did not provide any description or illustration, and two transmission electron micrographs (Dodge & Bibby, 1973) do not permit species identification. Taylor (1976) also described specimens as

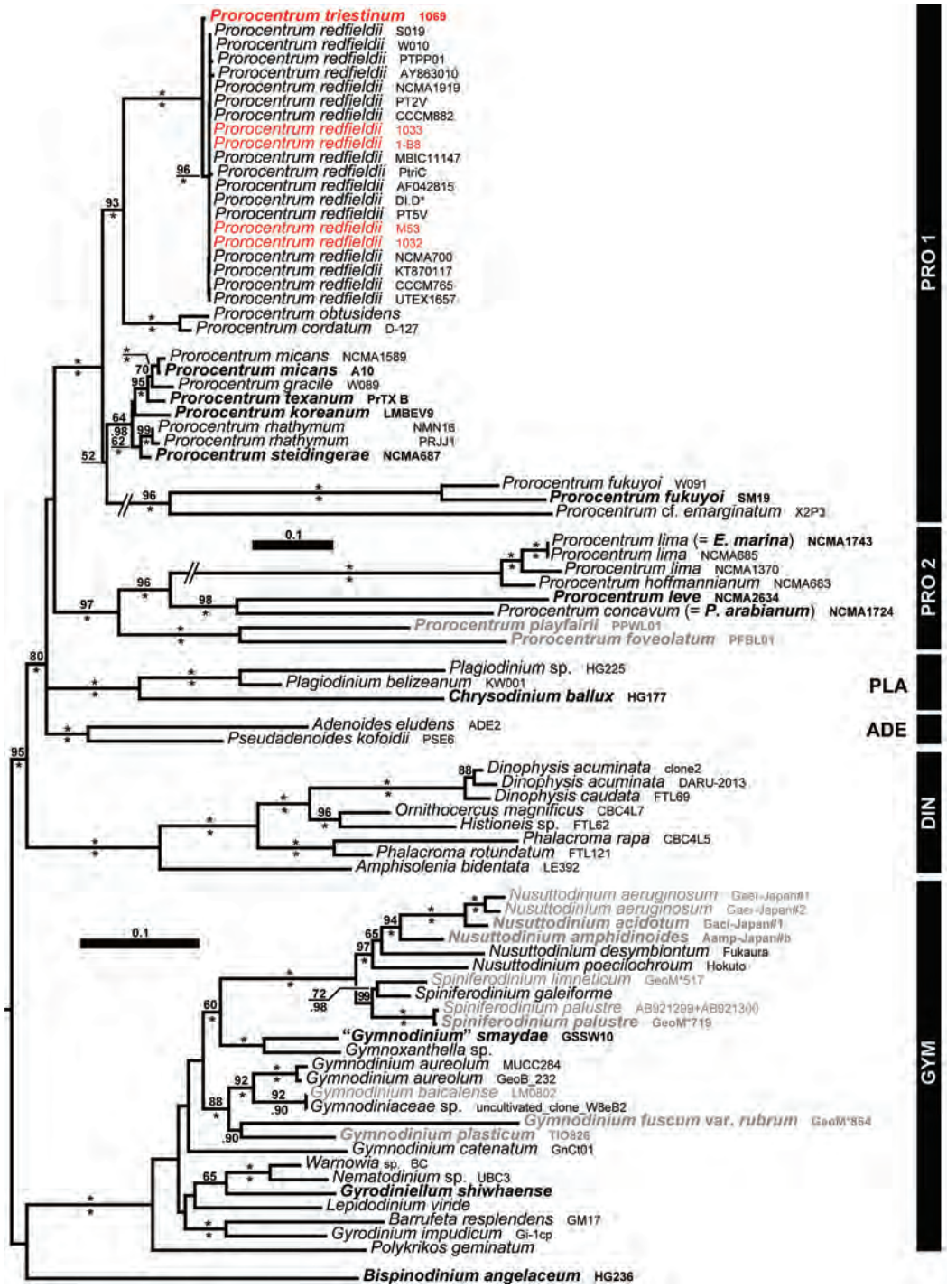

Fig. 79. A molecular tree of 42 systematically representative Prorocentrales, including all 21 accessions assignable to *Prorocentrum redfieldii* and *P. triestinum*. Maximum likelihood tree (–52 177.36), as inferred from a rRNA nucleotide alignment (1635 parsimony-informative sites) and with strain number information. Accessions corresponding to type or at least reference material are in bold type, freshwater accessions are in grey, and strains sequenced in this study are in red. Numbers on branches are ML bootstrap (above) and Bayesian support values (below) for the clusters (asterisks indicate maximal support values, values under 50 and 0.90, respectively, are not shown). Clades are indicated (abbreviations: ADE, *Adenoides*; DIN, Dinophysales; GYM, Gymnodiniales; PLA, *Plagiodinium*; PRO, *Prorocentrum*).

P. triestinum; they were in the correct size range and had smooth plates with the expected pattern of thecal pores, but the diagnostic spine was absent (Table 3). A record from Venezuela (Gamboa Márquez *et al.*, 1994) identified as *P.* cf. *triestinum* is likely also a misidentification and does not correspond to *P. redfieldii* either, because of differences in cell size (34–42 μm long), shape (oval in outline), spine length (8–15 μm) and pore number on thecal plates. On the other hand, light micrographs of cells labelled as *P. triestinum* by Shin *et al.* (2005: plate 2l, m) are fairly intermediate in shape and spine length between *P. triestinum* and *P. redfieldii* (Table 3) and warrant re-examination.

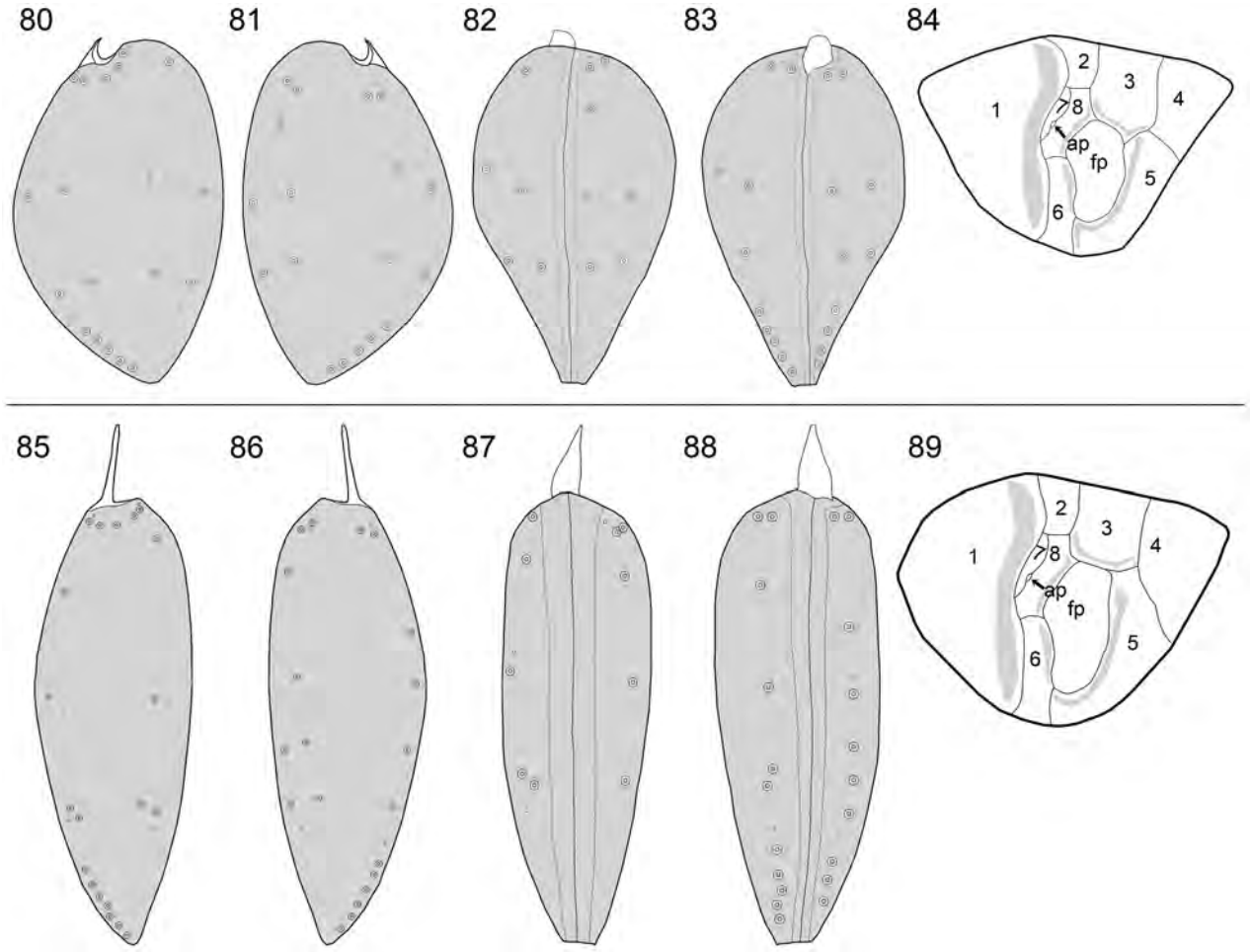

Figs 80–89. Schematic drawing including representative pore pattern and the periflagellar areas of *P. triestinum* (upper panel) and *P. redfieldii* (lower panel). **Figs 80, 85**. Right lateral view. **Figs 81, 86**. Left lateral view. **Figs 82, 87**. Ventral view. **Figs 83, 88**. Dorsal view. **Figs 84, 89**. Periflagellar area. ap, accessory pore; fp, flagellar pore.

One well-described species from Venice, *Prorocentrum venetum* Tolomio & Cavolo (Tolomio & Cavolo, 1985) is morphologically similar to *P. triestinum*, but the cells are only slightly asymmetric in shape (Table 3), and the posterior end is round. Like *P. triestinum*, the position of the apical spine and periflagellar area is dorso-subapical in position, the apical spine is very short (Table 3), and both share a similar basic pattern of thecal pores. *Prorocentrum venetum* is thus likely part of the *P. triestinum*/*P. redfieldii* lineage. Unfortunately, Tolomio & Cavolo (1985) did not compare their new species to *P. triestinum*, which was described from the nearby Trieste (Schiller, 1918). Re-investigation, including resolution of the periflagellar area, and molecular sequence diagnostics would help resolve the relationship between the two species.

Prorocentrum rhathymum A.R.Loeblich, Sherley & Schmidt is morphologically similar to *P. triestinum* and *P. venetum*, but it clearly differs from both by several morphological distinctions (Loeblich III *et al.*, 1979) that lead to different clade allocation in the phylogenetic tree (Fig. 79).

In conclusion, our study has importance for the reliable biodiversity assessment of dinophytes such as *Prorocentrum*. Future detailed studies of other similar species of *Prorocentrum* (e.g. *P. venetum* or taxa depicted by Böhm, 1936; Taylor, 1976; Shin *et al.*, 2005) may reveal an even higher diversity within this group than is known today.

Taxonomic activity

***Prorocentrum triestinum* J.Schiller**, Archiv für Protistenkunde 38: 252, fig. 1a–b. 1918.
TYPE: [non-fossil]: Mediterranean Sea, Adriatic Sea, off Italy: Friuli-Venezia Giulia, Trieste.
LECTOTYPE: designated here: [illustration] fig. 1b! in Schiller (1918; reproduced here as Fig. 1b).
EPITYPE: designated here: Mediterranean Sea, Adriatic Sea, off Italy: Friuli-Venezia Giulia, Trieste, Santa Croce, 19 September 2018: [SEM stub] A. Beran [A. Beran 1069] s.n. (CEDiT-2021E124!, isoepitypes: CEDiT-2021I125!). [http://phycobank.org/102715].

Table 3. Comparison of the diagnostic characters of *Prorocentrum triestinum, P. redfieldii*, the closely related species *P. venetum* and specimens attributed to *P. triestinum* by different authors.

	P. triestinum this study	*P. redfieldii* this study	*P. venetum* Tolomio & Cavolo (1985)	*P. triestinum sensu* Böhm (1936)	*P. triestinum sensu* Taylor (1976)	*P. triestinum sensu* Shin *et al.* (2005)
Size length [µm]	20.1–25.8	21.8–36.1	19.0–21.0	22-24	18.8–21-8	34.0[1]
depth [µm]	10.9–15.6	8.5–13.2	13.0–14.0		10.6–11.5	17.8
L/D ratio	1.76 (1.40–1.99)	2.85 (2.07–4.01)	ca. 1.5	ca. 2.5[2]	1.6–1.9	1.9
Asymmetry in lateral view	strong	weak	weak	weak	weak	weak
Posterior tip	acute (lateral) truncate (ventral)	acute (lateral) truncate (ventral	round (lateral) truncate (ventral)	acute (lateral) n.d. (ventral)	acute-round[3] n.d. (ventral)	acute (lateral) n.d. (ventral)
Apical spine	short (~1.5 µm) dorso-subapical	long (~5 µm) apical	short (~1.5 µm) slightly dorso-subapical	short (~2.2 µm*) apical	no spine	long (~5 µm) apical
Thecal plate surface	smooth	smooth	smooth	smooth	smooth	smooth
Pore arrangement	apical row; along sagittal suture	apical row; along sagittal suture	apical row; along sagittal suture	not examined	apical row; along sagittal suture	not examined
Pore number	12–21 large pores per plate	10–23 large pores per plate	30–40 (large) pores per plate	not examined	8–11 (presumably large pores) per plate	not examined
Periflagellar area	8 platelets reduced ap	8 platelets reduced ap	not examined	not examined	not examined	not examined
Schematic drawing (not to scale)[4]	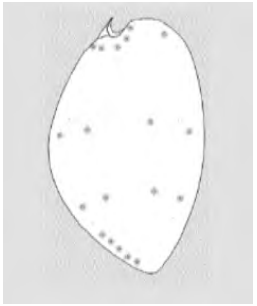	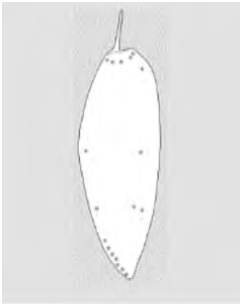	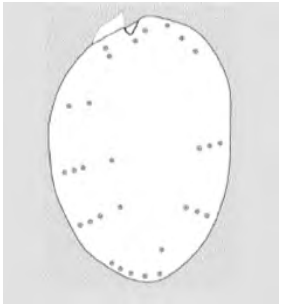	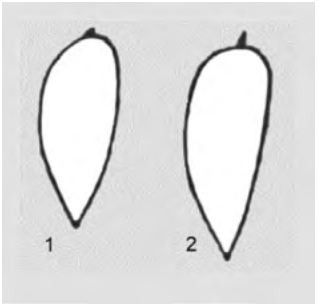	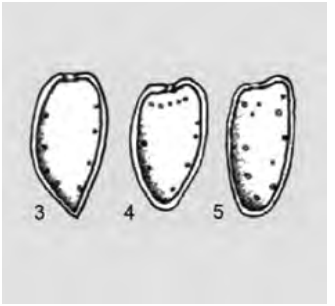	

[1]In their written description, Shin *et al.* (2005) reported cells being 20 ~ 30 µm long and 10 ~ 15 wide (i.e. deep in corrected terminology), but measuring the two cells in their Plate 2 l, m revealed the size reported here.
[2]Estimated from Fig. 3 b2 in Böhm (1936).
[3]The three cells depicted by Taylor (1976) may not represent the same species.
[4]The cells of *P. venetum* and *P. triestinum* sensu Shin *et al.* (2005), were drawn from cells depicted in the original publication. Drawings of *P. triestinum* sensu Böhm (1936) and of *P. triestinum* sensu Taylor (1976) are modified from the original publication.

Acknowledgements

MH thanks Nils Gülzow (Wilhelmshaven) for allocating his *P. redfieldii* strain from the German Bight. The authors are thankful to Dr Steve Pueppke (Michigan State University) for improving the English of this manuscript.

Disclosure statement

No potential conflict of interest was reported by the authors.

Funding

This work was supported by the PACES II research program of the Alfred-Wegener-Institute as part of the Helmholtz Foundation initiative in Earth and Environment.

Supplementary information

The following supplementary material is accessible via the Supplementary Content tab on the article's online page at https://doi.org/10.1080/09670262.2021.1948614

Supplementary table S1. Voucher list. All names are given under the rules of the ICN, the author standard forms follow Brummitt & Powell (1992). Abbreviation: n. inf., no information; s.n., without number. If 'holotype' or 'epitype' is noted for a species name, then it refers to material from which the type was prepared.

Supplementary figures S1–S12. *Prorocentrum redfieldii* (strain 1033) LM. **figs S1–S9**. Living cells. **figs S11**, **S12**. Formaldehyde-fixed cells. **figs S1–S9**. General size and shape of cells in right lateral (figs S1, S2), in left lateral (figs S3, S4), in ventral (figs S5, S9) and in dorsal (figs S6–S8) view. Note the long apical trichocyst rods (arrows in figs S1, S7), the thick chromosomes (visible, e.g., in figs S1, S4, S7, S8), the presence of thecal pores (arrows) visible for the empty theca in fig. S10 and the presumptive pusule (p) in fig. S8. **fig. S11**. Cell with blue light excitation, when chlorophyll autofluorescence indicated chloroplast structure. **fig. S12**. DAPI stained cell with UV excitation to illustrate shape and position of the nucleus. Scale bars: 5 µm.

Supplementary figures S13–S20. *Prorocentrum redfieldii* (strain 1033) SEM, entire cells. **fig. S13**. Cell in right lateral view. **fig. S14**. Cell in left lateral view. **fig. S15**. Cell in left-lateral ventral view. **figs S16**, **S17**. Cells in ventral view. **fig. S18**. Cell in right-lateral dorsal view. **figs S19**, **S20**. Cells in dorsal view. Scale bars: 5 µm.

Supplementary figures S21–S242. *Prorocentrum redfieldii* (strain 1033), detailed SEM of surface structure, pores and of the periflagellar area. **figs S21**, **S22**. Large tubular and small pores in external (fig. S21) and internal (fig. S22) view. Note the presence of a mini-pore located posterior at the antapex (white arrow in fig. S21), which is distinctly smaller than a small pore (black arrow in fig. S21). **figs S23**, **S24**. Detailed view of the periflagellar area of the same cell in two different magnifications. ap = accessory pore, fp = flagellar pore. Scale bars: 1 µm.

Author contributions

U. Tillmann: original concept, isolation of strains, morphological analysis and discussion, drafting and editing manuscript. A. Beran: isolation of strains, morphological discussion, editing manuscript; M. Gottschling: phylogenetic analysis, drafting and editing manuscript; S. Wietkamp, DNA extraction and sequencing, editing manuscript; M. Hoppenrath: original concept, morphological discussion, drafting and editing manuscript.

ORCID

Urban Tillmann http://orcid.org/0000-0002-8207-4382
Alfred Beran http://orcid.org/0000-0003-3723-4161
Marc Gottschling http://orcid.org/0000-0002-4381-8051
Stephan Wietkamp http://orcid.org/0000-0001-7516-9861

References

Adachi, M., Sake, Y. & Ishida, Y. (1996). Analysis of *Alexandrium* (Dinophyceae) species using sequences of the 5.8S ribosomal DNA and internal transcribed spacer regions. *Journal of Phycology*, **32**: 424–432.

Adachi, R. (1972). A taxonomical study of the red tide organisms. *Journal of Faculty of Fisheries, Prefectural University of Mie*, **9**: 9–145.

Agatha, S., Strüder-Kypke, M.C. & Beran, A. (2004). Morphological and genetic variability in the marine planktonic ciliate *Laboea strobila* Lohmann, 1908 (Ciliophora, Oligotrichia), with notes on its ontogenesis. *Journal of Eukaryotic Microbiology*, **51**: 267–281.

Altschul, S.F., Gish, W., Miller, W., Myers, E.W. & Lipman, D.J. (1990). Basic logical alignment search tool. *Journal of Molecular Biology*, **215**: 403–410.

Berney, C., Ciuprina, A., Bender, S., Brodie, J., Edgcomb, V., Kim, E., Rajan, J., Parfrey, L.W., Adl, S., Audic, S., Bass, D., Caron, D.A., Cochrane, G., Czech, L., Dunthorn, M., Geisen, S., Glöckner, F.O., Mahé, F., Quast, C., Kaye, J.Z., Simpson, A.G.B., Stamatakis, A., del Campo, J., Yilmaz, P. & de Vargas, C. (2017). UniEuk: time to speak a common language in protistology! *Journal of Eukaryotic Microbiology*, **64**: 407–11.

Böhm, A. (1936). Dinoflagellates of the coastal waters of the Western Pacific. *Bulletin of the Bernice P. Bishop Museum*, **137**: 1–54.

Braarud, T. & Rossavik, E. (1951). Observations on the marine dinoflagellate *Prorocentrum micans* Ehrenb. in culture. *Avhandlinger Norske Videnskaps-Akadademi i Oslo. I. Matematisk-Naturvidenskapelig Klasse*, **1**: 318.

Bursa, A.S. (1959). The genus *Prorocentrum* Ehrenberg. Morphodynamics, protoplasmic structure, and taxonomy. *Canadian Journal of Botany*, **37**: 1–31.

Bursa, A.S. (1962). Some morphogenetic factors in taxonomy of dinoflagellates. *Grana Palynologica*, **3**: 54–66.

Cabrini, M. & Strami, F. (2006). *Prorocentrum triestinum* Schiller 1918. In *Guida al riconoscimento del plancton dei mari italiani, volume I – Fitoplancton*. (Avancini, M., Cicero, A.M., Di Girolamo, I., Innamorati, M., Magaletti, E. & Sertorio Zunini, T., editors). Ministero dell'Ambiente della Tutela del Territorio e del Mare – DPN, ICRAM – Istituto Centrale per la Ricerca scientifica e tecnologica Applicata al Mare.

Chomérat, N., Bilien, G. & Zentz, F. (2019). A taxonomical study of benthic *Prorocentrum* species (Prorocentrales, Dinophyceae) from Anse Dufour (Martinique Island, eastern Caribbean Sea). *Marine Biodiversity*, **49**: 1299–1319.

Dodge, J.D. (1965). Thecal fine-structure in the dinoflagellate genera *Prorocentrum* and *Exuviaella*. *Journal of the Marine Biological Association of the United Kingdom*, **45**: 607–614.

Dodge, J.D. (1975). The Prorocentrales (Dinophyceae). II. Revision of the taxonomy within the genus *Prorocentrum*. *Botanical Journal of the Linnean Society*, **71**: 103–125.

Dodge, J.D. (1982). *The Dinoflagellates of the British Isles*. Her Majesty´s Stationery Office, London.

Dodge, J.D. & Bibby, B.T. (1973). The Prorocentrales (Dinophyceae) I. A comparative account of fine structure in the genera *Prorocentrum* and *Exuviaella*. *Botanical Journal of the Linnean Society*, **67**: 175–187.

Dodge, J.D. & Crawford, R.M. (1970). A survey of thecal fine structure in the Dinophyceae. *Botanical Journal of the Linnean Society*, **63**: 53–67.

Elfering, S., Wohlrab, S., Neuhaus, S., Cembella, A., Harms, L. & John, U. (2020). Comparative metabarcoding and metatranscriptomic analysis of microeukaryotes within coastal surface waters of West Greenland and Northwest Iceland. *Frontiers in Marine Science*, **7**: 439.

Gamboa Márquez, J., Sánchez Suárez, I. & La Barbera Sánchez, A. (1994). Dinoflagelados (Pyrrhophyta) del archipiélago los Roques (Venezuela): familias Prorocentraceae y Ostreopsidaceae/Dinoflagellates (Pyrrhophyta) from the los Roques archipielago (Venezuela): families Prorocentraceae and Ostreopsidaceae. *Acta Cientifica Venezolana*, **45**: 140–152.

Gottschling, M., Chacón, J., Žerdoner Čalasan, A., Neuhaus, S., Kretschmann, J., Stibor, H. & John, U. (2020). Phylogenetic placement of environmental sequences using taxonomically reliable databases helps to rigorously assess dinophyte biodiversity in Bavarian lakes (Germany). *Freshwater Biology*, **65**: 193–208.

Hada, Y. (1975). On two new species of the genus *Prorocentrum* Ehrenberg belonging to Dinoflagellida. *Hiroshima Shudo Daigaku Ronshu*, **16**: 31–38.

Heil, C.A., Glibert, P.M. & Fan, C. (2005). *Prorocentrum minimum* (Pavillard) Schiller: a review of a harmful algal bloom species of growing worldwide importance. *Harmful Algae*, **4**: 449–470.

Hernández-Becerril, D.U., Cortéz Altamirano, R. & Alonso, R.R. (2000). The dinoflagellate genus *Prorocentrum* along the coasts of the Mexican Pacific. *Hydrobiologia*, **418**: 111–121.

Hoppenrath, M. (2004). A revised checklist of planktonic diatoms and dinoflagellates from Helgoland (North Sea, German Bight). *Helgoland Marine Research*, **58**: 243–251.

Hoppenrath, M., Chomérat, N., Horiguchi, T., Schweikert, M., Nagahama, Y. & Murray, S. (2013). Taxonomy and phylogeny of the benthic *Prorocentrum* species (Dinophyceae) – a proposal and review. *Harmful Algae*, **27**: 1–28.

Hoppenrath, M., Elbrächter, M. & Drebes, G. (2009). *Marine Phytoplankton. Selected Microphytoplankton Species from the North Sea around Helgoland and Sylt*. Schweizerbart, Stuttgart.

Hoppenrath, M., Murray, S., Chomérat, N. & Horiguchi, T. (2014). Marine Benthic Dinoflagellates – Unveiling their Worldwide Biodiversity. Kleine Senckenberg-Reihe, Band 54, Schweiterbart.

Katoh, K. & Standley, D.M. (2013). MAFFT Multiple sequence alignment software version 7: improvements in performance and usability. *Molecular Biology and Evolution*, **30**: 772–780.

Keller, M.D., Selvin, R.C., Claus, W. & Guillard, R.R.L. (1987). Media for the culture of oceanic ultraphytoplankton. *Journal of Phycology*, **23**: 633–638.

Kretschmann, J., Žerdoner Čalasan, A., Kusber, W.-H. & Gottschling, M. (2018). Still curling after all these years: *Glenodinium apiculatum* Ehrenb. (Peridiniales, Dinophyceae) repeatedly found at its type locality in Berlin (Germany). *Systematics and Biodiversity*, **16**: 200–209.

Loeblich III, A.R., Sherley, J.L. & Schmidt, R.J. (1979). The correct position of flagellar insertion in *Prorocentrum* and description of *Prorocentrum rhathymum* sp. nov. (Pyrrhophyta). *Journal of Plankton Research*, **1**: 113–120.

Lu, D. & Goebel, J. (2001). Five red tide species in genus *Prorocentrum* including the description of *Prorocentrum donghaiense* Lu sp. nov. from the east China Sea. *Chinese Journal of Oceanology and Limnology*, **19**: 337–344.

Medlin, L., Elwood, H.J., Stickel, S. & Sogin, M.L. (1988). The characterization of enzymatically amplified eukaryotic 16S-like rRNA-coding regions. *Gene*, **71**: 491–499.

Miller, M.A., Pfeiffer, W. & Schwartz, T. (2010). Creating the CIPRES Science Gateway for inference of large phylogenetic trees. In *Proceedings of the Gateway Computing Environments Workshop* (*GCE*) 1–8. New Orleans.

Mora, D., Abarca, N., Proft, S., Grau, J.H., Enke, N., Carmona, J., Skibbe, O., Jahn, R. & Zimmermann, J. (2019). Morphology and metabarcoding: a test with stream diatoms from Mexico highlights the complementarity of identification methods. *Freshwater Science*, **38**: 448–464.

Ndhlovu, A., Dhar, N., Garg, N., Xuma, T., Pitcher, G.C., Sym, S.D. & Durand, P.M. (2017). A red tide forming dinoflagellate *Prorocentrum triestinum*: identification, phylogeny and impacts on St Helena Bay, South Africa. *Phycologia*, **56**: 649–665.

Nilsson, R.H., Ryberg, M., Kristiansson, E., Abarenkov, K., Larsson, K.-H. & Kõljalg, U. (2006). Taxonomic reliability of DNA sequences in public sequence databases: a fungal perspective. *PLoS ONE*, **1**: e59.

Okamoto, K. (1992). Dinoflagellates found in Hamana lake. I. Genus *Prorocentrum*. *Bulletin of the Plankton Society of Japan*, **38**: 121–133.

Paulsen, O. (1908). XVIII. Peridiniales. In *Nordisches Plankton* (Brandt, K. & Apstein, C., editors), 1–124. Lipsius & Tischer, Kiel.

Ronquist, F., Teslenko, M., Van Der Mark, P., Ayres, D.L., Darling, A., Höhna, S., Larget, B., Liu, L., Suchard, M.A. & Huelsenbeck, J.P. (2012). MrBayes 3.2: efficient Bayesian phylogenetic inference and model choice across a large model space. *Systematic Biology*, **61**: 539–542.

Schiller, J. (1918). Über neue *Prorocentrum*- und *Exuviaella*-Arten aus der Adria. *Archiv für Protistenkunde*, **38**: 250–262.

Schiller, J. (1928). Die planktische Vegetationen des adriatischen Meeres. C. Dinoflagellata I Teil. Adiniferidae, Dinophysidaceae. *Archiv für Protistenkunde*, **61**: 46–91.

Schiller, J. (1933). Dinoflagellatae (Peridineae) in monographischer Behandlung. In *Dr. L. Rabenhorst´s Kryptogamen-Flora von Deutschland, Österreich und der Schweiz*. (Kolkwitz, R., editor) 1–615. Akademische Verlagsgesellschaft, Leipzig.

Schiller, J. (1937). Dinoflagellatae (Peridineae) in monographischer Behandlung. In *Dr. L. Rabenhorst´s Kryptogamen-Flora von Deutschland, Österreich und der Schweiz* (Rabenhorst, L., editor), 1–590. Johnson, New York.

Scholin, C.A., Herzog, M., Sogin, M. & Anderson, D.M. (1994). Identification of group- and strain-specific genetic markers for globally distributed *Alexandrium* (Dinophyceae). II.

Sequence analysis of a fragment of the LSU rRNA gene. *Journal of Phycology*, **30**: 999–1011.

Shin, E.Y., Yeo, H.G. & Park, J.G. (2005). Morphological re-examination of *Prorocentrum* spp. in Korean coastal waters. *Korean Journal of Environmental Biology*, **23**: 184–190.

Shin, H.H., Li, Z., Mertens, K.N., Seo, M.H., Gu, H., Lim, W.A., Yoon, Y.H., Soh, H.Y. & Matsuoka, K. (2019). *Prorocentrum shikokuense* Hada and *P. donghaiense* Lu are junior synonyms of *P. obtusidens* Schiller, but not of *P. dentatum* Stein (Prorocentrales, Dinophyceae). *Harmful Algae*, **89**: 101686.

Stamatakis, A. (2014). RAxML version 8: a tool for phylogenetic analysis and post-analysis of large phylogenies. *Bioinformatics*, **30**: 1312–1313.

Taylor, F.J.R. (1976). Dinoflagellates from the International Indian Ocean 1976 Expedition. *Bibliotheca Botanica*, **132**: 1–234.

Throndsen, J. (1983). *Ultra- and Nanoplankton Flagellates from Coastal Waters of Southern Honshu and Kyushu, Japan (including some results from the western part of the Kuroshiwo off Honshu)*. Research Department, Fisheries Agency, Japan; Gakujutsu Tosho, Tokyo.

Tillmann, U., Hoppenrath, M. & Gottschling, M. (2019). Reliable determination of *Prorocentrum micans* Ehrenb. (Prorocentrales, Dinophyceae) based on newly collected material from the type locality. *European Journal of Phycology*, **54**: 417–431.

Tillmann, U., Trefault, N., Krock, B., Parada-Pozo, G., De La Iglesia, R. & Vásquez, M. (2017). Identification of *Azadinium poporum* (Dinophyceae) in the Southeast Pacific: morphology, molecular phylogeny, and azaspiracid profile characterization. *Journal of Plankton Research*, **39**: 350–367.

Tolomio, C. & Cavolo, F. (1985). Description de *Prorocentrum venetum* sp. nov. (Dinophyceae) trouvé dans la Lagune de Venise. *Botanica Marina*, **28**: 345–349.

Toriumi, S. (1980). *Prorocentrum* species (Dinophyceae) causing red tide in Japanese coastal waters. *Bulletin of the Plankton Society of Japan*, **27**: 105–112.

Velikova, V. & Larsen, J. (1999). The *Prorocentrum cordatum*/*Prorocentrum minimum* taxonomic problem. *Grana*, **38**: 108–112.

Yasumoto, T., Seino, N., Murakami, Y. & Murata, M. (1987). Toxins produced by benthic dinoflagellates. *Biological Bulletin*, **172**: 128–131.

Yoo, K.I. & Lee, J.B. (1986). Taxonomical studies on dinoflagellates in Masa Bay. 1. Genus *Prorocentrum* Ehrenberg. *Journal of the Oceanological Society of Korea*, **21**: 46–55.